

1 **Title**

2 Quiescent center initiation in the *Arabidopsis* lateral root primordia is dependent on the
3 *SCARECROW* transcription factor

4

5 **Running title**

6 QC establishment in lateral root

7

8 **Authors**

9 Tatsuaki Goh^{1,2,†,*}, Koichi Toyokura¹, Darren M. Wells², Kamal Swarup², Mayuko
10 Yamamoto¹, Tetsuro Mimura¹, Dolf Weijers³, Hidehiro Fukaki¹, Laurent Laplace⁴,
11 Malcolm J. Bennett², Soazig Guyomarc'h^{5,*}

12

13 **Affiliations**

14 ¹ Department of Biology, Graduate School of Science, Kobe University, Kobe 657-8501,
15 Japan

16 ² Centre for Plant Integrative Biology, University of Nottingham, Nottingham LE12 5RD,
17 United Kingdom

18 ³ Laboratory of Biochemistry, Wageningen University, Wageningen, The Netherlands

19 ⁴ Institut de Recherche pour le Développement, Unité Mixte de Recherche (UMR)
20 Diversité Adaptation et Développement des plantes (DIADE), 34394 Montpellier Cedex
21 5, France

22 ⁵ Université de Montpellier, Unité Mixte de Recherche (UMR) Diversité Adaptation et

23 Développement des plantes (DIADE), 34394 Montpellier Cedex 5, France

24 ‡ Present address: Graduate School of Biological Sciences, Nara Institute of Science and
25 Technology, 8916-5 Takayama, Ikoma, Nara, 630-0192 Japan

26

27 ***Corresponding authors**

28 Tatsuaki Goh

29 Department of Biology, Graduate School of Science, Kobe University

30 1-1 Rokkodai, Kobe 657-8501 Japan

31 Phone: +81-78-803-5721

32 E-mail: goh@bs.naist.jp

33

34 Soazig Guyomarc'h

35 “Diversity, Adaptation and Development of Plants” Research unit,

36 Institute of Research for Development and University of Montpellier

37 911 avenue Agropolis, F-34090 Montpellier, France

38 Phone: +33-467416462

39 E-mail: soazig.guyomarch@ird.fr

40

41 **Keywords**

42 lateral root organogenesis, quiescent center, *SCARECROW*, 3D live imaging,

43 *Arabidopsis thaliana*

44

45 **Summary statement**

46 Live 3D imaging revealed *de novo* establishment of organizing center cells (quiescent
47 center) in *Arabidopsis* lateral root primordia is dependent on *SCARECROW* expression
48 and coincides with a developmental phase transition.

49

50 **Abstract**

51 Lateral root (LR) formation is an important determinant of root system architecture. In
52 *Arabidopsis*, LRs originate from pericycle cells, which undergo a programme of
53 morphogenesis to generate a new LR meristem. Despite its importance for root meristem
54 organisation, the onset of organizing center (termed quiescent center; QC) formation
55 during LR morphogenesis remains unclear. Here, we used live 3D confocal imaging to
56 monitor cell organization and identity acquisition during LR development. Our dynamic
57 observations revealed an early morphogenesis phase and a late meristem formation phase
58 as proposed in the bi-phasic growth model described by Sussex and co-workers. LR QC
59 establishment coincided with this developmental phase transition. QC precursor cells
60 originated from the outer layer of stage II LR primordia, within which the *SCARECROW*
61 (*SCR*) transcription factor was specifically expressed. Disrupting *SCR* function abolished
62 periclinal divisions in this LR primordia cell layer and perturbed the formation of QC
63 precursor cells. We conclude that *de novo* QC establishment in LR primordia operates via
64 *SCR*-mediated formative cell division and coincides with the developmental phase
65 transition.

66

67 **Introduction**

68 The plasticity of plant root system architecture provided by post-embryonic lateral root
69 (LR) formation greatly contributes to its adaptability to environmental conditions (Bao et
70 al., 2014). LRs facilitate nutrient and water acquisition by increasing soil exploration.
71 While primary root initiation, organization and growth have been extensively studied, the
72 molecular and cellular mechanisms that control the patterning of new lateral root
73 primordia (LRPs) are still poorly characterized (Tian et al., 2014a). Root growth results
74 from the activity of the root apical meristem (RAM), a group of proliferating cells
75 organized around a central stem cell niche (SCN). The RAM of the primary root is
76 created during early embryogenesis through formative cell divisions and initial cell
77 identity is maintained by an organizing center termed the quiescent center (QC; Perilli et
78 al., 2012; ten Hove et al., 2015). A number of regulatory mechanisms have been
79 identified that control QC establishment and maintenance in the primary root, especially
80 in the model plant *Arabidopsis thaliana*. The phytohormone auxin controls the
81 specification of the hypophysis (the QC precursor cell) during embryogenesis and later
82 maintains QC function in seedling roots with the AP2-domain *PLETHORA* (*PLT*)
83 transcription factors (Moller and Weijers, 2009; ten Hove et al., 2015). The maintenance
84 of the QC and SCN during post-embryonic primary root growth relies on the activity of
85 *PLT* and GRAS-family transcription factors *SHORT-ROOT* (*SHR*) and *SCARECROW*
86 (*SCR*) in combination with an auxin gradient (Bennett and Scheres, 2010; Perilli et al.,
87 2012).

88 Despite similarities between primary and lateral root meristems, these

89 structures are generated in different tissue and genetic contexts, and many of the
90 processes governing the generation of a new root meristem in LRP remains to be
91 elucidated (Lavenus et al., 2013; Tian et al., 2014a). In particular, little is known about the
92 patterning processes controlling *de novo* establishment of the QC and SCN in the
93 developing LRP (Laskowski et al., 1995; Tian et al., 2014a). In *A. thaliana*, LRs originate
94 from a subset of ~ 6 pericycle cells that divide and form a new root apical meristem with
95 a radially symmetrical structure akin to the PR (Lavenus et al., 2013). A pioneering study
96 of *Arabidopsis* lateral root development by Ian Sussex and co-workers originally
97 proposed that LR organogenesis occurs in two successive steps: first, an early
98 morphogenesis phase during which a primordium composed of 3 to 5 layers of
99 approximately isodiametric cells is generated; second, a meristem formation phase,
100 during which cell identity patterning and meristem organization occurs, generating the
101 characteristic tissue structure of the root apex (Laskowski et al., 1995). Later, Malamy
102 and Benfey (1997) performed an extensive analysis of LRP morphogenesis and proposed
103 eight developmental stages (termed Stage I to VII and emergence) based on anatomical
104 criteria and these structural milestones have been confirmed in later studies (Lucas et al.,
105 2013; von Wangenheim et al., 2016). In summary, LRP formation is initiated when
106 asymmetric anticlinal cell divisions of founder cells produce pairs of abutting small cells
107 flanked by longer cells (stage I; Goh et al., 2012). Next, the central smaller cells undergo
108 three further rounds of periclinal cell divisions to create a four-layered primordium
109 (Stages II–IV). During stages V and VI, the LRP acquires a cellular organization similar
110 to the primary RAM. At the emergence stage, the LRP finally breaks through overlying

111 root tissues and enters the soil (Lavenus et al., 2013; Malamy and Benfey, 1997). Thus, an
112 anatomical organisation reminiscent of a presumptive organizing center was first
113 observed in longitudinal sections of stage VI lateral root primordia. However, the
114 dynamics of QC establishment during LRP development has remained elusive (Tian et al.,
115 2014a).

116 Here, we investigated further the classical two-step LRP developmental model
117 formulated by Sussex and co-workers (Laskowski et al., 1995) , focusing on the
118 mechanisms controlling *de novo* QC formation during LRP development. We developed
119 a 3D time-lapse confocal laser scanning microscopy imaging approach to analyse
120 development of living lateral root primordia. We observed that QC formation, as reported
121 by QC marker gene expression, occurs at the transition between the early morphogenesis
122 phase and the later meristem organization phase of LRP development. These two events
123 also coincide with a 3D organ shape change from bilateral to radial. Cell lineage analysis
124 revealed that the QC originates from the outer layer of stage II LRP. We report that the
125 GRAS family transcription factor *SCR* regulates QC formation by controlling formative
126 periclinal cell divisions that give rise to QC precursor cells. We conclude that *de novo* QC
127 establishment in LR depends on *SCR* expression in the outer layer of stage II primordia
128 and coincides with a developmental phase transition.

129

130 **Results**

131 **LR formation exhibits a bi-phasic pattern of growth**

132 To understand the molecular and cellular mechanisms controlling LR organogenesis, a
133 confocal laser scanning microscopy (CLSM)-based 3D time-lapse imaging approach was
134 developed using a transgenic line ubiquitously expressing a plasma membrane-localized
135 yellow fluorescent protein (YFP)-tagged reporter termed WAVE131Y (Geldner et al.,
136 2009). Images were taken at 10 min intervals as Z stacks (2 μ m step) over a 24-hour
137 period. This strategy allowed us to observe the entire process of LRP morphogenesis
138 spanning from early developmental stages up to organ emergence at high temporal and
139 spatial resolution and was compatible with the monitoring of live functional cell markers.
140 Precise analysis of time-lapse 3-D image series of developing LRP obtained using this
141 method was consistent with the 2-D anatomical stages described by Malamy and Benfey
142 (1997). Importantly, our imaging technique also allowed us to explore the kinetics of LRP
143 morphogenesis throughout these stages (Fig. 1A, B and Movie 1). Following anticlinal
144 divisions of founder cells creating a one-layered stage I primordium, later periclinal
145 divisions generate a two-layered LRP (stage II, Fig. 1A t = 0:00), which subsequently
146 undergo new anticlinal divisions to produce a stage II primordium composed of small
147 cells (Fig. 1A t = 4:00, white arrowheads). A second round of periclinal cell divisions in
148 the outer layer of stage II (Fig. 1A t = 7:00, white arrowhead) then creates a three-layered
149 primordium (termed stage III). A third round of periclinal divisions (this time in the
150 innermost cell layer) produces a four-layered LRP (termed stage IV, Fig. 1A t = 9:30,
151 white arrowhead). In summary, during this early morphogenesis phase (stage I to IV),

152 well-coordinated anticlinal and periclinal cell divisions generate a four-layered LRP.
153 Stage V was characterized by anticlinal divisions at the flanking cells of outer layers (Fig.
154 1A t = 14:00, arrowheads) and elongation of inner cells (Fig. 1A t = 14:00 and 15:00,
155 denoted by two-directional arrows). Stage VI LRP exhibited periclinal and anticlinal cell
156 divisions that produced the endodermal and cortical layers, and periclinal cell divisions in
157 the outermost layer that will give rise to the root cap (Figs. 1A t = 21:00, arrowheads, S1).
158 Thus, through characteristic cell divisions and cell elongation events in stage V and VI,
159 an anatomically recognisable meristematic structure is formed as early as stage VI,
160 consistently with what Malamy and Benfey (1997) initially described.

161 During the early LRP morphogenesis phase (stages I to IV), cell divisions
162 remained constrained within the space between underlying protoxylem and overlying
163 endodermal tissues (Fig. 1A, B). Both protoxylem and endodermal cells contain lignified
164 walls (termed the Casparian strip in the latter case) that provide these tissues with
165 structural rigidity (Naseer et al., 2012). These rigid cell walls, especially the Casparian
166 strip, provide mechanical constraints on LRPs, which impact the LRP morphogenesis
167 (Lucas et al., 2013; Vermeer et al., 2014). Consistent with this, our time-lapse image data
168 revealed that the rate of organ outgrowth (inferred from changes in its height) remained
169 slow until stage V (Fig. 1C), and LRP shape was flattened when the LRP was passing
170 through the endodermal layer (Fig. 1A t = 7:00, 9:30 and 14:00). Then, the growth rate of
171 LRP significantly accelerated (Fig. 1C), and LRP changed to dome-shaped from the end
172 of stage V (meristem formation phase; Fig. 1A t = 15:00) (Kumpf et al., 2013; Lucas et al.,
173 2013). This expansion of the LRP seems principally caused by axial elongation of cells at

174 the base of the primordium (depicted by two-directional arrows in Fig. 1A, t = 14:00 and
175 15:00).

176 Taken together, these time-lapse observations of developing primordia
177 suggested that LRP formation operates in two developmental phases: an early
178 morphogenesis phase (stage I – IV) during which a four-layered LRP is formed,
179 constrained between the xylem pole and the endodermis, and a later meristem formation
180 phase (stage V onwards) characterized by the onset of a mature meristem structure and
181 rapid organ outgrowth. This is consistent with the hypothesis that LRP formation is a
182 bi-phasic growth process as originally proposed by Laskowski *et al.* (1995), with phase
183 transition occurring at stage V as described by Malamy and Benfey (1997).

184

185 **3D cell division orientation and LRP shape change coincides with a developmental** 186 **phase transition**

187 We previously reported that LRPs initially exhibit bilateral symmetry that later changes
188 to radial symmetry, adopting a cylindrical shape similar to the primary root (Lucas et al.,
189 2013). Tangential divisions at the flanking side contribute to the 3D LRP shape change by
190 creating a ring of cells surrounding the central dividing cells (Lucas et al., 2013). In order
191 to better understand the contribution of division plane orientation to the 3D LRP shape
192 and its relationship with the LRP developmental phase transition, we monitored nuclear
193 dynamics employing our time lapse imaging system with a nuclear-localized reporter line
194 termed *pRPS5a::H2B:tdTomato* (Adachi et al., 2011) and then tracked LRP nuclei
195 movement and cell divisions (Figs. 2A–F, S2). 4D-nuclei tracking showed the

196 contributions of daughter cells derived from pericycle cell files adjacent to the xylem pole
197 in the 3D LRP structure, and revealed that LRPs are predominantly formed from cells in
198 three files of pericycle cells (Fig. 2A–F, Movie 2). Consistent with previous analysis
199 (Kurup et al., 2005; von Wangenheim et al., 2016), the central pericycle file provided all
200 of the cells in the central median plane (green), whilst cells derived from adjacent
201 pericycle files (red and orange) contributed to the LRP flanks (Fig. 2A–F, Movie 2). Until
202 stage IV, cells from the central cell file underwent three rounds of periclinal cell division
203 to create a four-layered primordium (t = 12:00, Fig. 2A, B). Around the phase transition
204 (Stage V, t = 16:00, Fig. 2C, D, Movie 2), an abrupt reorientation of the cell division plane
205 (termed longitudinal) occurred in the median file of the LRP, contributing to primordium
206 widening (t = 22:00, Fig. 2E, F, white arrows). Careful analysis of cell division patterns in
207 WAVE131Y-expressing LRP revealed that new longitudinal planes of cell divisions
208 indeed promoted LRP widening at stage V (Fig. 1E, tangential sections [d, e],
209 arrowheads). Hence, cell division plane re-orientation at stage V contributes to 3D LRP
210 shape change towards a cylindrical structure, concomitant with the early-to-late LRP
211 morphogenesis phase transition. Thus a developmental transition takes place at stage V
212 during LRP development, and encompasses two events: the change from an early 4-layer
213 primordium generation phase to a later meristem organization phase, and a switch from
214 bilateral to radial organ growth.

215

216 **QC formation occurs simultaneously with a LRP developmental transition at stage**

217 **V**

218 In the primary root, QC cells function as an organizing center regulating the activity and
 219 maintenance of the stem cell niche (SCN; Bennett and Scheres, 2010; Perilli et al., 2012).
 220 Despite its fundamental importance for meristem formation and subsequent growth of
 221 new LRAs, nothing is known about the spatio-temporal regulation of post-embryonic
 222 formation of QC cells. To address this, we initially studied the expression dynamics of the
 223 QC-specific reporter line *QC25::CFP* (ten Hove et al., 2010) using our time-lapse
 224 imaging system. *QC25::CFP* expression was first detected in cells at the center of the
 225 second outermost layer at stage IV/V, and the reporter signal was enhanced at later stage
 226 (Fig. 1A–E, Movie 1). The expression of *QC25::CFP* was initiated before the
 227 characteristic cell divisions and accelerated organ outgrowth at the later meristem
 228 formation phase (Fig. 1A, C, Movie 1).
 229 To confirm this observation and explore how QC formation is related to 3D structural
 230 changes of the LRP, we performed nuclear tracking in developing primordia expressing
 231 both *pWOX5::n3GFP* and *pRPS5a::H2B::tdTomato* markers (Fig. 2G–Z, Movie 3). The
 232 second QC marker *pWOX5::n3GFP* exhibited an identical spatial and temporal
 233 expression pattern to *QC25::CFP* in the LRP (Figs. 1, 2G–K, Movies 1, 3), initially being
 234 detected in the central cells of the second outermost layer of stage IV/V just prior to phase
 235 transition ($t = 14:00$, Fig. 2I, N, S, X). Importantly, the longitudinal divisions occurred
 236 simultaneously with expression of *WOX5* (Fig. 2J, O, T, Y, Movie 4) and *QC25::CFP*
 237 (Fig. 1E). Digital cross-sections revealed that the expression of both QC reporters was
 238 detected in a subset of four LRP cells located in the center of the second outermost layer
 239 of stage V primordia (Figs. 1E, tangential section [e], 2O, P, T, U, Y, Z, Movie 4),

240 suggesting that the central single cell file produced a group of four QC cells by
241 reorientation of cell division plane (i.e. longitudinally) at stage V. Based on the timing of
242 induction of both *QC25* and *WOX5* markers, we conclude that QC establishment
243 coincides with the developmental transition from an initial basic cellular organization
244 with bilateral symmetry to the later meristem formation phase with progressive
245 acquisition of radial symmetry.

246

247 **QC cells originate from the outer layer of stage II LRP**

248 To help determine how the QC is established during the earlier stages of development, we
249 tracked cell lineages in developing LRP using our time-lapse series of CLSM images (Fig.
250 1B). Our analysis revealed that vascular and pericycle tissues originated from the inner
251 layer of stage II LRP (indicated by pink in Fig. 1B), whereas the outer layer of stage II
252 LRP gave rise to the epidermis, ground tissues (endodermis and cortex) and root cap
253 tissues (shown in light blue in Figs. 1B, S1). Our dynamic cell-fate analysis validated the
254 lineage model proposed by Malamy and Benfey (1997). In addition, our analysis revealed
255 that QC cells are derived from the outer layer of stage II LRP. More precisely the central
256 daughter cells of the second outermost layer, after the second periclinal division of the
257 outer layer of stage II LRP, were specified as QC precursor cells, in which the expression
258 of QC markers was initiated at stage V (Fig. 1A, B, QC cells are shown in dark blue in Fig.
259 1B). Hence, the differentiation of inner and outer layers in the stage II LRP appears to be
260 an important event preceding QC specification and subsequent root meristem patterning.

261

262 ***SHR* and *SCR* expression domains distinguish inner and outer LRP layers**

263 Earlier studies have reported that the GRAS-type transcription factor *SCARECROW*
264 (*SCR*) is one of the earliest genes exhibiting differential LRP expression, specifically in
265 the outer layer of stage II primordia (Malamy and Benfey, 1997). *SCR* interacts with
266 another GRAS-type transcription factor, *SHORT-ROOT* (*SHR*), to regulate SCN
267 maintenance, ground tissue formation and organ growth in the PR (Fisher and Sozzani,
268 2015). Using our time-lapse imaging system, a functional *pSCR::GFP:SCR* marker (in a
269 *scr-3* mutant background (Gallagher et al., 2004)) was first detected in stage II LRP
270 specifically in the outer layer (Fig. 3A t = 4:00 and 8:00, F, Movie 5). Following periclinal
271 division of the outer layer of stage II LRP, the GFP:SCR protein was initially detected in
272 both daughter cell layers (Fig. 3A t = 12:00, G), but the signal gradually disappeared from
273 the outermost layer (Fig. 3A t = 16:00), while it was maintained in the nuclei of cells
274 within the second outermost layer of the LRP after stage III (Fig. 3A t = 20:00, H). The
275 second outermost layer-specific expression of the *SCR* gene was confirmed using a
276 transcriptional *pSCR:GUS:GFP* reporter (Fig. 3C–E). Consistent with previous reports
277 (Malamy and Benfey, 1997; Tian et al., 2014b), our dynamic live confocal observations
278 revealed how the *SCR*-expression domain forms during LRP development.

279 *SCR* transcription is largely dependent on *SHR* (Helariutta et al., 2000;
280 Levesque et al., 2006). In primary RAMs, the *SHR* gene is expressed in stele cells
281 (including the pericycle) where the SHR protein is localized in the cytosol and nucleus,
282 but the SHR protein moves via plasmodesmata to nuclei of adjacent QC and endodermal
283 cells, where it activates *SCR* expression (Nakajima et al., 2001). In stage I LRP, the

functional SHR:GFP protein expressed under the control of its own regulatory region (*pSHR::SHR:GFP*) in the *shr-2* mutant background (Nakajima et al., 2001) was detected very weakly in all cells (Fig. 3B, Movies 6, 7 t = 0:00). In stage II LRP, the SHR:GFP protein signal gradually increased in cells of the inner layer while it was weakly detected in the outer layer (Fig. 3B t = 4:00 and 8:00) where the SHR:GFP proteins locate in the nucleus (Fig. 3B, L). From stage III onwards, the SHR:GFP protein signal remained high in the inner layer-derived tiers, and gradually increased in the nuclei of cells of the second outermost layer directly overlying *SHR*-expressing inner layer-derived cells (Fig. 3B t = 12:00–20:00, M, N, Movies 6, 7). The inner layer-specific expression of the *SHR* gene was confirmed using a transcriptional *pSHR:GUS* reporter (Fig. 3I–K), consistent with published results (Lucas et al., 2011). The appearance of SHR:GFP protein in cell nuclei in the second outermost layer of the LRP coincided with an enhanced level of GFP:SCR signal in those cells (Fig. 3A, B), consistent with *SCR* transcription being largely *SHR* dependent (Helariutta et al., 2000; Levesque et al., 2006). Thus, our imaging system helped refine our knowledge of *SCR* and *SHR* expression dynamics in developing primordia and revealed that in stage II LRP the *SHR* and *SCR* transcriptional domains demark the inner and outer cell layers respectively, which might be functionally important for further primordium morphogenesis.

302

303 **The *scr* mutation disrupts QC establishment**

304 To determine the functional importance of *SCR* outer layer-specific expression in stage II
305 primordia, we analysed LRP morphogenesis in the *scr-3* mutant using time-lapse imaging

306 (Figs. 4 and 5). In wild-type plants, periclinal divisions in stage II LRPs occurred
307 according to a regular sequence: cells divided initially in the outer layer, and
308 subsequently in the inner layer (Fig. 1A, t = 7:00 and 9:30, Movie 1). After stage II
309 periclinal division, two or three rounds of cell divisions were observed in the outermost
310 layer-derived cells in the following 20 hours (Figs. 5A, blue box and nuclei, S3). Slower
311 divisions were observed in the cells derived from the second outermost layer of stage IV
312 in the same time period (Figs. 5A, red box and nuclei, S3). In contrast, cell divisions in
313 the outer layer of the *scr-3* mutant LRPs were largely abolished during early primordia
314 development (Fig. 4A, B, t = 6:00, Movie 8), while the inner layer underwent periclinal
315 divisions. Later, cell divisions in the outer layer-derived tiers of the primordium occurred
316 only once in a small number of central cells during the 20 hours of our time-lapse
317 observation, although inner layer-derived cells continued to divide in a wild-type fashion
318 (Figs. 4A, B, t = 11:30 and 18:00, 5B, S3, Movie 8). As a consequence, after stage II, it is
319 difficult to assign precise stages to developing *scr-3* primordia according to Malamy and
320 Benfey's nomenclature. Hence, *SCR* appears to promote the second round of periclinal
321 cell divisions in the outer layer of the stage II LRP, as well as subsequent divisions of the
322 outer layer derivatives, whereas inner layer cell divisions are independent of *SCR*
323 function.

324 In order to confirm the specific cell division defects in the outer layer of the
325 *scr-3* mutant, we monitored the spatial activity of the *SCR* promoter (*pSCR::GUS:GFP*)
326 during LRP development. Whilst *pSCR::GUS:GFP* signal was clearly enhanced in the
327 second outermost layer of WT LRPs at stage V (Fig. 4C, D), it appeared more uniform in

328 *scr-3* cells derived from presumptive derivatives of stage II-outermost layer at
329 approximately the same stage (Fig. 4E, F). We also observed similar defects in the
330 periclinal cell division in the outer layer and spatial pattern of *SCR* promoter activity in
331 *shr-2* (Fig. S4), consistent with the mutant's previously reported severe LRP patterning
332 defects (Lucas et al., 2011). These observations suggested that defects in periclinal
333 divisions in the stage-II outermost layer of *scr-3* and *shr-2* LRP disrupt the correct spatial
334 regulation of *SCR* expression during later LRP development. Based on these data, we
335 conclude that periclinal divisions in the outer layer of stage II LRP (some of which
336 generated the future QC cells) are regulated by *SCR* and *SHR*.

337 Our earlier cell lineage analysis revealed that the periclinal divisions in the
338 outer layer of the stage II LRP are important for producing QC precursor cells (Fig. 1A,
339 B). Thus, disrupting periclinal cell division in the outer layer of the *scr-3* stage II LRP
340 would compromise QC formation. Indeed, nuclear expression of the *pWOX5::n3GFP*
341 QC marker was undetectable in the *scr-3* mutant LRP prior to organ emergence (Fig. 6).
342 At 24 h, WOX5 promoter activity was weakly detected at a QC-like position, after which
343 reporter expression was strongly detected at later time points (Fig. 6). This observation
344 suggested that specific expression of *SCR* in the outer layer of stage II promotes
345 formative periclinal cell divisions to produce QC precursor cells and subsequent QC
346 establishment in the LRP.

347 Nevertheless, *scr-3* LRP continued to develop as a result of the division of cells
348 derived from the inner layer, and eventually cells occupying similar positions to
349 wild-type QC cells in *scr-3* LR expressed the *pWOX5::n3GFP* marker, albeit

350 considerably later than the wild type (Fig. 6, t = 28:30 and 34:00, indicated by red
351 arrowheads). Consistent with this observation, the *scr* mutant created mature LRs,
352 although they were shorter than those of WT (Fig. S5), possibly due to later defects in
353 SCN maintenance by similar mechanisms to the PR (Sabatini et al., 2003). Interestingly,
354 tracking the origin of the QC marker-positive cells in the *scr-3* mutant revealed that they
355 were derived from inner layer cells of the stage II LRP (Fig. 6B, shown in pink). Our
356 observations suggest that QC formation in the LRP is normally dependent on
357 *SCR*-mediated periclinal cell division in the outer layer of the stage II LRP. However,
358 when the normal pattern of QC establishment is defective, QC cells still eventually
359 establish, albeit independent of *SCR* regulation via a distinct LRP cell lineage.
360

361 **Discussion**

362 LR formation represents a highly integrated and dynamic process that transforms LR
363 founder cells into new root meristems. Here, we describe *de novo* establishment of QC
364 and meristem organization during LRP morphogenesis. A 3D time-lapse confocal
365 imaging approach revealed that LRP development operates in a bi-phasic manner: first,
366 from stage I to IV, periclinal and anticlinal cell divisions create a simple four-layered
367 primordium with respect to the main growth axes of pericycle cells. From stage V
368 onwards, more complex cell division patterning contributes to meristem formation
369 accompanied with accelerated growth and 3D shape change to a radially cylindrical
370 structure similar to the PR. Our time-lapse analyses of live LRP development are
371 consistent with previously reported results (Laskowski et al., 1995; Malamy and Benfey,
372 1997), and further support the model of a biphasic morphogenesis process initially
373 proposed by Laskowski et al. (1995) (Fig. 7).

374 Our confocal-based time-lapse imaging system allowed us to analyse live
375 lateral root development with high spatio-temporal resolution. This approach is
376 complementary to the light sheet fluorescent microscopy (LSFM)-based imaging
377 technique reported by von Wangenheim and co-workers (2016). Both techniques enable
378 4D monitoring of living lateral root primordia. While LSFM offers 4D visualisation of
379 the root sample with reduced exposure to laser sources, our confocal-based approach
380 provides advantages such as high-resolution and flexible control of multi-coloured
381 imaging, by enabling visualization of multiple reporters simultaneously.

382 Our study also revealed that the transition between the two major phases of
383 LRP development, namely early morphogenesis phase and late meristem formation phase,
384 occurs in stage V primordia and coincides with the onset of QC marker gene expression
385 in central cells of the second outermost layer. Despite previously reported observations
386 suggesting earlier onset of *WOX5* expression during LR development (Ditengou et al.,
387 2008), our repeated analyses of two new QC markers (*pWOX5::n3GFP* and *QC25::CFP*)
388 support the conclusion that QC identity is established around stage V during LRP
389 development.

390 Our study also reveals that QC establishment in LRs relies on the
391 differentiation of the inner and outer layers in stage II primordia controlled by two
392 GRAS-family transcription factors, *SCR* (outer layer) and *SHR* (inner layer). It is
393 plausible that, as observed in the primary root meristem, SHR protein movement from the
394 presumptive stele of stage II primordium to the overlying cell layer induces *SCR*
395 expression and that SCR-SHR interaction later restricts *SCR* expression domain to the
396 second outermost layer of the developing LRP (Cui et al., 2007). However, the precise
397 mechanisms regulating *SHR* expression, migration and transcriptional activity in the
398 context of lateral root development remain to be elucidated.

399 The *SCR*-expressing outer LRP layer produces QC precursor cells via
400 *SCR*-regulated periclinal cell divisions. These observations are reminiscent of two
401 functional properties of SCN regulation in the primary root. First, *WOX5* expression in
402 the PR meristem was shown to depend on the SCR/SHR regulation pathway (Sarkar et al.,
403 2007). Thus, despite the differences in the tissue context of both events, regulation of

404 *WOX5* expression by the SHR/SCR module seems to be conserved between primary and
405 lateral root meristem formation. Second, earlier work on the primary root has shown that
406 *SHR* and *SCR* regulate formative cell divisions in root ground tissue initial cells,
407 generating endodermal and cortical layers (Cruz-Ramirez et al., 2012; Sozzani et al.,
408 2010). In this study, we report that in stage II LR primordia, SCR also regulates the
409 formative periclinal division of the outer layer, preceding QC specification. This suggests
410 that cell division pattern for QC establishment is regulated differently during LR
411 development and embryogenesis in *Arabidopsis* (Wysocka-Diller et al., 2000) and that,
412 while SCR is not strictly required for LR QC establishment, “normal” QC-forming
413 formative divisions in the lateral root primordium depends on SCR function.

414 Ian Sussex and co-workers originally proposed that the formation of a LR
415 meristem is a two-step process (Laskowski et al., 1995), and hypothesized that there is an
416 unknown developmental transition event between these two phases. We report that QC
417 formation correlates with the transition from an early morphogenesis phase to a later
418 meristem formation phase at stage V, and with bilateral to radial 3D organ shape change.
419 Before that stage, the SCR/SHR module controls the initial inner/outer patterning of stage
420 II primordium and promotes the formative periclinal cell division of the outer layer that
421 precedes QC formation. After that stage, QC specification might contribute to orchestrate
422 further steps of root meristem organization in the developing primordium. Primary root
423 QC cells organize SCN activity and maintenance through controlling phytohormone
424 distribution and the spatio-temporal activity of transcription factors (Perilli et al., 2012;
425 ten Hove et al., 2015). It will be interesting to analyse how QC establishment influences

426 meristem organization and maintenance in the second phase of LRP development, and to
427 compare it to the regulatory networks operating in the primary root apex. Interestingly,
428 despite being severely impaired in outer layer-derived cell divisions during the earlier
429 developmental phase, ultimately the *scr* mutant could still establish a QC at a similar
430 position to the WT. This observation suggests that cells in the early LRP of the *scr* mutant
431 still have competency for QC establishment, which might have similar regulatory
432 mechanisms to root regeneration (Sena et al., 2009; Xu et al., 2006). This emphasizes the
433 robustness of LR meristem patterning mechanisms with respect to cell lineage. We
434 hypothesize that QC cell specification in the LR is regulated by yet to be determined
435 positional information (e.g., phytohormones, mobile signals) and a dynamic gene
436 regulatory network (Lavenus et al., 2015; Voss et al., 2015). Further analyses will help to
437 address the SCR-independent patterning mechanisms for *de novo* QC specification in the
438 LRP and shed light on the functional importance of this new stem cell niche for LRP
439 development.

440 **Materials and Methods**

441 **Plant materials and growth conditions**

442 The *A. thaliana* accession Col-0 was used throughout the experiments. The following
443 transgenic plants were used: *QC25::CFP* (ten Hove et al., 2010), *WAVE131Y* (Geldner et
444 al., 2009), *pRPS5a::H2B:tdTomato* (Adachi et al., 2011), *pSCR::GFP:SCR* (*scr-3*)
445 (Gallagher et al., 2004), *pSHR::SHR:GFP* (*shr-2*) (Nakajima et al., 2001), *pSHR::GUS*
446 (Helariutta et al., 2000), *shr-2* and *scr-3* (Fukaki et al., 1998) and *AUX1-YFP* (Swarup et
447 al., 2004). Seeds were germinated under sterile conditions on 1x Murashige-Skoog
448 medium solidified with 0.5% gellan gum containing 0.5 g/L MES-KOH (pH 5.8), 0.01%
449 *myo*-inositol and 1% sucrose. Plants were grown at 23°C under continuous light in
450 vertically orientated petri dishes.

451

452 **Vector construction and plant transformation**

453 To generate *pSCR::GUS:GFP*, In-Fusion Cloning (TaKaRa) was used to clone a *SCR*
454 promoter fragment (2,349 bp) amplified by PCR with the primers
455 pGWB-XbaI-AtSCRpro-F
456 (GCAGGTCGACTCTAGAGACCGGAGAGAGACCGGAGAA) and
457 pGWB-XbaI-AtSCRpro-R
458 (TGTTGATAACTCTAGAGTTGGTCGTGAGATTGCATGGT) into pGWB550
459 (Nakagawa et al., 2007). A *GUS* fragment amplified by PCR with the primers
460 attB1-F-GUS (aaaaagcaggetCCATGGTCCGTCCTGTAGAAAC) and attB2-R-GUS
461 (agaaagctgggtATTGTTTGCCTCCCTGCTGCG) was cloned into pDONR221 and

462 transferred into pGWB550-AtSCRpro by the Gateway technology (Life Technology). To
463 generate *pWOX5::n3GFP*, an approximately 4.6-kb fragment of the upstream region of
464 *WOX5* was amplified as described previously (Sarkar et al., 2007), and then cloned
465 upstream of SV40-3xGFP in pGreenIIKAN (Takada and Jurgens, 2007). The plasmid
466 was introduced into Col-0 by the floral dip transformation method (Clough and Bent,
467 1998).

468

469 **Time-lapse imaging of LR morphogenesis**

470 For time-lapse imaging, 5-day-old plants were placed horizontally into a
471 cover-glass-bottom chamber (Thermo Fisher) with a block of solid medium and observed
472 under an inverted confocal microscope (Leica SP5II or Olympus FV1000 with a Z focus
473 drift compensating system (ZDC)). In order to allow plant growth on the microscope
474 stage during image acquisition, a LED lighting system was coupled to the microscope
475 hardware. On the Leica SP5II, an USB relay controller (KMtronic) and countdown timer
476 software custom-written in the LabVIEW development environment (National
477 Instruments) turned off the light during laser scanning. For the Olympus FV1000, a
478 ring-shaped LED lamp attached to the microscope condenser was controlled by the TTL
479 signal output from the FV1000. Images were taken every 10 or 15 minutes at 2 μ m
480 Z-steps using a 60x water immersion objective lens with immersion medium Immersol W
481 2010 (Zeiss), and then processed with the Image J program Fiji (Schindelin et al., 2012)
482 and its plugin Correct 3D drift (http://fiji.sc/Correct_3D_drift) for the registration of
483 3D+T image dataset. Each observation was repeated at least three times. For the cell

484 lineage map, confocal images were traced by the CellSet software (Pound et al., 2012),
485 and then drawn by Illustrator (Adobe). The divisions and movements of nuclei labelled
486 with *pRPS5a::H2B:tdTomato* (Adachi et al., 2011) were tracked with TrackMate (ver.
487 2.7.4) on the software Fiji (<http://fiji.sc/TrackMate>).

488

489 **GFP observation and GUS staining**

490 For GFP observation with a confocal microscope (Olympus FV1000), roots were
491 counterstained with propidium iodide (PI, 10 µg/ml). For GUS staining, roots were
492 prefixed with ice-cold 90% acetone for 15 min, and then stained with GUS staining
493 solution (100 mM sodium phosphate, pH 7.0, 10 mM EDTA, 5 mM potassium
494 ferrocyanide, 5 mM potassium ferricyanide, 0.1% Triton X-100 and 0.5 mg/ml
495 5-bromo-4-chloro-3-indoyl-β-D-glucuronide (X-Gluc)). Whole-mount clearing
496 preparation of roots was performed using chloral hydrate. Samples were observed with a
497 Leica DM6000 microscope equipped with Nomarski optics (Leica Microsystems).

498

499 **Acknowledgments**

500 We thank Philip N Benfey (Duke Univ.), Ben Scheres (Wageningen UR), Sachihito
501 Matsunaga (Tokyo Univ. of Sci.) and Tsuyoshi Nakagawa (Shimane Univ.) for providing
502 experimental materials. We also thank Yuichiro Imai (Olympus Corp.) for providing
503 valuable advice and technical support for the time-lapse imaging and lighting system, and
504 Yoshie Okamoto and Shiori Sera for technical assistance.

505

506 **Competing interests**

507 The authors declare no competing or financial interests.

508

509 **Author contributions**

510 T.G., L.L., M.J.B. and S.G. designed the research; T.G. and K.S. performed the research;

511 T.G., K.T., D.M.W., M.Y., T.M., D.W. H.F. and S.G. contributed new tools; T.G., L.L.,

512 M.J.B. and S.G. analyzed the data; T.G., K.T., H.F., L.L., M.J.B. and S.G. wrote the

513 paper; all authors read and approved the paper.

514

515 **Funding**

516 This work was supported by the Ministry of Education, Culture, Sports, Science and

517 Technology (MEXT) through a JSPS Research Fellowship for Young Scientists (No.

518 12J02079 to T.G.), a Grant-in-Aid for Scientific Research on Priority Areas (No.

519 19060006 to H.F.), and a Grant-in-Aid for Scientific Research on Innovative Areas (No.

520 25113003 to H.F.).

521

522 **References**

- 523 **Adachi, S., Minamisawa, K., Okushima, Y., Inagaki, S., Yoshiyama, K., Kondou, Y.,**
524 **Kaminuma, E., Kawashima, M., Toyoda, T., Matsui, M., et al. (2011).**
525 Programmed induction of endoreduplication by DNA double-strand breaks in
526 *Arabidopsis*. *Proc. Natl. Acad. Sci. USA* **108**, 10004-10009.
- 527 **Bao, Y., Aggarwal, P., Robbins, N. E., Sturrock, C. J., Thompson, M. C., Tan, H. Q.,**
528 **Tham, C., Duan, L., Rodriguez, P. L., Vernoux, T., et al. (2014).** Plant roots
529 use a patterning mechanism to position lateral root branches toward available
530 water. *Proc. Natl. Acad. Sci. USA* **111**, 9319-9324.
- 531 **Bennett, T. and Scheres, B. (2010).** Root development-two meristems for the price of
532 one? *Curr Top Dev Biol* **91**, 67-102.
- 533 **Clough, S. J. and Bent, A. F. (1998).** Floral dip: a simplified method for
534 *Agrobacterium*-mediated transformation of *Arabidopsis thaliana*. *Plant J.* **16**,
535 735-743.
- 536 **Cruz-Ramirez, A., Diaz-Trivino, S., Blilou, I., Grieneisen, V. A., Sozzani, R.,**
537 **Zamioudis, C., Miskolczi, P., Nieuwland, J., Benjamins, R., Dhonukshe, P., et**
538 **al. (2012).** A bistable circuit involving SCARECROW-RETINOBLASTOMA
539 integrates cues to inform asymmetric stem cell division. *Cell* **150**, 1002-1015.
- 540 **Cui, H., Levesque, M. P., Vernoux, T., Jung, J. W., Paquette, A. J., Gallagher, K. L.,**
541 **Wang, J. Y., Blilou, I., Scheres, B. and Benfey, P. N. (2007).** An evolutionarily
542 conserved mechanism delimiting SHR movement defines a single layer of
543 endodermis in plants. *Science* **316**, 421-425.

544 **Ditengou, F. A., Teale, W. D., Kochersperger, P., Flittner, K. A., Kneuper, I., van der**
545 **Graaff, E., Nziengui, H., Pinoso, F., Li, X., Nitschke, R., et al. (2008).**
546 Mechanical induction of lateral root initiation in *Arabidopsis thaliana*. *Proc. Natl.*
547 *Acad. Sci. USA* **105**, 18818-18823.

548 **Fisher, A. P. and Sozzani, R. (2015).** Uncovering the networks involved in stem cell
549 maintenance and asymmetric cell division in the *Arabidopsis* root. *Curr. Opin.*
550 *Plant Biol.* **29**, 38-43.

551 **Fukaki, H., Wysocka-Diller, J., Kato, T., Fujisawa, H., Benfey, P. N. and Tasaka, M.**
552 (1998). Genetic evidence that the endodermis is essential for shoot gravitropism
553 in *Arabidopsis thaliana*. *Plant J.* **14**, 425-430.

554 **Gallagher, K. L., Paquette, A. J., Nakajima, K. and Benfey, P. N. (2004).** Mechanisms
555 regulating SHORT-ROOT intercellular movement. *Curr. Biol.* **14**, 1847-1851.

556 **Geldner, N., Denervaud-Tendon, V., Hyman, D. L., Mayer, U., Stierhof, Y. D. and**
557 **Chory, J. (2009).** Rapid, combinatorial analysis of membrane compartments in
558 intact plants with a multicolor marker set. *Plant J.* **59**, 169-178.

559 **Goh, T., Joi, S., Mimura, T. and Fukaki, H. (2012).** The establishment of asymmetry in
560 *Arabidopsis* lateral root founder cells is regulated by LBD16/ASL18 and related
561 LBD/ASL proteins. *Development* **139**, 883-893.

562 **Helariutta, Y., Fukaki, H., Wysocka-Diller, J., Nakajima, K., Jung, J., Sena, G.,**
563 **Hauser, M. T. and Benfey, P. N. (2000).** The *SHORT-ROOT* gene controls radial
564 patterning of the *Arabidopsis* root through radial signaling. *Cell* **101**, 555-567.

565 **Kumpf, R. P., Shi, C. L., Larrieu, A., Sto, I. M., Butenko, M. A., Peret, B., Riiser, E.**

566 **S., Bennett, M. J. and Aalen, R. B.** (2013). Floral organ abscission peptide IDA
567 and its HAE/HSL2 receptors control cell separation during lateral root emergence.
568 *Proc. Natl. Acad. Sci. USA* **110**, 5235-5240.

569 **Kurup, S., Runions, J., Köhler, U., Laplace, L., Hodge, S. and Haseloff, J.** (2005).
570 Marking cell lineages in living tissues. *Plant J.* **42**, 444-453.

571 **Laskowski, M. J., Williams, M. E., Nusbaum, H. C. and Sussex, I. M.** (1995).
572 Formation of lateral root meristems is a two-stage process. *Development* **121**,
573 3303-3310.

574 **Lavenus, J., Goh, T., Guyomarc'h, S., Hill, K., Lucas, M., Voss, U., Kenobi, K.,**
575 **Wilson, M. H., Farcot, E., Hagen, G., et al.** (2015). Inference of the Arabidopsis
576 lateral root gene regulatory network suggests a bifurcation mechanism that
577 defines primordia flanking and central zones. *Plant Cell* **27**, 1368-1388.

578 **Lavenus, J., Goh, T., Roberts, I., Guyomarc'h, S., Lucas, M., De Smet, I., Fukaki, H.,**
579 **Beeckman, T., Bennett, M. and Laplace, L.** (2013). Lateral root development in
580 *Arabidopsis*: fifty shades of auxin. *Trends Plant Sci.* **18**, 450-458.

581 **Levesque, M. P., Vernoux, T., Busch, W., Cui, H., Wang, J. Y., Blilou, I., Hassan, H.,**
582 **Nakajima, K., Matsumoto, N., Lohmann, J. U., et al.** (2006). Whole-genome
583 analysis of the SHORT-ROOT developmental pathway in *Arabidopsis*. *PLoS Biol.*
584 **4**, e143.

585 **Lucas, M., Kenobi, K., von Wangenheim, D., Vobeta, U., Swarup, K., De Smet, I.,**
586 **Van Damme, D., Lawrence, T., Peret, B., Moscardi, E., et al.** (2013). Lateral
587 root morphogenesis is dependent on the mechanical properties of the overlaying

588 tissues. *Proc. Natl. Acad. Sci. USA* **110**, 5229-5234.

589 **Lucas, M., Swarup, R., Paponov, I. A., Swarup, K., Casimiro, I., Lake, D., Peret, B.,**
590 **Zappala, S., Mairhofer, S., Whitworth, M., et al.** (2011). Short-Root regulates
591 primary, lateral, and adventitious root development in *Arabidopsis*. *Plant Physiol.*
592 **155**, 384-398.

593 **Malamy, J. E. and Benfey, P. N.** (1997). Organization and cell differentiation in lateral
594 roots of *Arabidopsis thaliana*. *Development* **124**, 33-44.

595 **Moller, B. and Weijers, D.** (2009). Auxin control of embryo patterning. *Cold Spring*
596 *Harb. Perspect. Biol.* **1**, a001545.

597 **Nakagawa, T., Suzuki, T., Murata, S., Nakamura, S., Hino, T., Maeo, K., Tabata, R.,**
598 **Kawai, T., Tanaka, K., Niwa, Y., et al.** (2007). Improved Gateway binary
599 vectors: high-performance vectors for creation of fusion constructs in transgenic
600 analysis of plants. *Biosci. Biotechnol. Biochem.* **71**, 2095-2100.

601 **Nakajima, K., Sena, G., Nawy, T. and Benfey, P. N.** (2001). Intercellular movement of
602 the putative transcription factor SHR in root patterning. *Nature* **413**, 307-311.

603 **Naseer, S., Lee, Y., Lapierre, C., Franke, R., Nawrath, C. and Geldner, N.** (2012).
604 Casparian strip diffusion barrier in *Arabidopsis* is made of a lignin polymer
605 without suberin. *Proc. Natl. Acad. Sci. USA* **109**, 10101-10106.

606 **Perilli, S., Di Mambro, R. and Sabatini, S.** (2012). Growth and development of the root
607 apical meristem. *Curr. Opin. Plant Biol.* **15**, 17-23.

608 **Pound, M. P., French, A. P., Wells, D. M., Bennett, M. J. and Pridmore, T. P.** (2012).
609 CellSeT: novel software to extract and analyze structured networks of plant cells

610 from confocal images. *Plant Cell* **24**, 1353-1361.

611 **Sabatini, S., Heidstra, R., Wildwater, M. and Scheres, B.** (2003). SCARECROW is
612 involved in positioning the stem cell niche in the *Arabidopsis* root meristem.
613 *Genes Dev.* **17**, 354-358.

614 **Sarkar, A. K., Luijten, M., Miyashima, S., Lenhard, M., Hashimoto, T., Nakajima,**
615 **K., Scheres, B., Heidstra, R. and Laux, T.** (2007). Conserved factors regulate
616 signalling in *Arabidopsis thaliana* shoot and root stem cell organizers. *Nature* **446**,
617 811-814.

618 **Schindelin, J., Arganda-Carreras, I., Frise, E., Kaynig, V., Longair, M., Pietzsch, T.,**
619 **Preibisch, S., Rueden, C., Saalfeld, S., Schmid, B., et al.** (2012). Fiji: an
620 open-source platform for biological-image analysis. *Nat. Methods* **9**, 676-682.

621 **Sena, G., Wang, X., Liu, H. Y., Hofhuis, H. and Birnbaum, K. D.** (2009). Organ
622 regeneration does not require a functional stem cell niche in plants. *Nature* **457**,
623 1150-1153.

624 **Sozzani, R., Cui, H., Moreno-Risueno, M. A., Busch, W., Van Norman, J. M.,**
625 **Vernoux, T., Brady, S. M., Dewitte, W., Murray, J. A. and Benfey, P. N.**
626 (2010). Spatiotemporal regulation of cell-cycle genes by SHORTROOT links
627 patterning and growth. *Nature* **466**, 128-132.

628 **Swarup, R., Kargul, J., Marchant, A., Zadik, D., Rahman, A., Mills, R., Yemm, A.,**
629 **May, S., Williams, L., Millner, P., et al.** (2004). Structure-function analysis of
630 the presumptive *Arabidopsis* auxin permease AUX1. *Plant Cell* **16**, 3069-3083.

631 **Takada, S. and Jurgens, G.** (2007). Transcriptional regulation of epidermal cell fate in

632 the *Arabidopsis* embryo. *Development* **134**, 1141-1150.

633 **ten Hove, C. A., Lu, K. J. and Weijers, D.** (2015). Building a plant: cell fate
634 specification in the early *Arabidopsis* embryo. *Development* **142**, 420-430.

635 **ten Hove, C. A., Willemsen, V., de Vries, W. J., van Dijken, A., Scheres, B. and**
636 **Heidstra, R.** (2010). *SCHIZORIZA* encodes a nuclear factor regulating
637 asymmetry of stem cell divisions in the *Arabidopsis* root. *Curr. Biol.* **20**, 452-457.

638 **Tian, H., De Smet, I. and Ding, Z.** (2014a). Shaping a root system: regulating lateral
639 versus primary root growth. *Trends Plant Sci.* **19**, 426-431.

640 **Tian, H., Jia, Y., Niu, T., Yu, Q. and Ding, Z.** (2014b). The key players of the primary
641 root growth and development also function in lateral roots in *Arabidopsis*. *Plant*
642 *Cell Rep* **33**, 745-753.

643 **Vermeer, J. E., von Wangenheim, D., Barberon, M., Lee, Y., Stelzer, E. H., Maizel, A.**
644 **and Geldner, N.** (2014). A spatial accommodation by neighboring cells is
645 required for organ initiation in *Arabidopsis*. *Science* **343**, 178-183.

646 **von Wangenheim, D., Fangerau, J., Schmitz, A., Smith, R. S., Leitte, H., Stelzer, E.**
647 **H. and Maizel, A.** (2016). Rules and Self-Organizing Properties of
648 Post-embryonic Plant Organ Cell Division Patterns. *Curr. Biol.* **26**, 439-449.

649 **Voss, U., Wilson, M. H., Kenobi, K., Gould, P. D., Robertson, F. C., Peer, W. A.,**
650 **Lucas, M., Swarup, K., Casimiro, I., Holman, T. J., et al.** (2015). The circadian
651 clock rephases during lateral root organ initiation in *Arabidopsis thaliana*. *Nat.*
652 *Commun.* **6**, 7641.

653 **Wysocka-Diller, J. W., Helariutta, Y., Fukaki, H., Malamy, J. E. and Benfey, P. N.**

654 (2000). Molecular analysis of SCARECROW function reveals a radial patterning
655 mechanism common to root and shoot. *Development* **127**, 595-603.

656 **Xu, J., Hofhuis, H., Heidstra, R., Sauer, M., Friml, J. and Scheres, B.** (2006). A
657 molecular framework for plant regeneration. *Science* **311**, 385-388.

658

659

660 **Figure legends**

661 **Fig. 1. Cellular patterning and QC establishment during *Arabidopsis* LR**
662 **primordium development.**

663 (A) Time-lapse image series of LR primordium development visualized using
664 WAVE131Y (plasma membrane, yellow) and QC25::CFP (QC marker, cyan). White
665 arrowheads and two-directional arrows indicate the characteristic cell divisions and cell
666 elongation, respectively. The elapsed time (h:min) after the start of observation and
667 developmental stage are indicated on each panel. See also Movie 1. Scale bar = 50 μ m.

668 (B) Cell lineage map of the LRP in A. The inner and outer layers of stage II (t = 0:00) are
669 shown in light blue and pink, respectively. The cells derived from each layer are indicated
670 by the same color. Dark blue indicates outer layer-derived cells that showed a QC25::CFP
671 signal.

672 (C) Quantification of LRP height (blue) and QC25::CFP fluorescence intensity (red).
673 QC25::CFP intensity was quantified at the center cells of the second outermost layer. LRP
674 developmental stages are categorized according to a previous paper (Malamy and Benfey,
675 1997).

676 (D, E) Front view (a, b, d and e) and top-down view (c and f) of digitally sliced images of
677 A (t = 9:30 (D) and 14:00 (E)). The white dotted lines in the side view images indicate the
678 positions of the sliced planes. White arrowheads indicate the longitudinal radial cell
679 divisions at the outermost (d) or second outermost layer (e) of the stage V LRP (E, t =
680 14:00). Scale bars = 50 μ m.

681

682 **Fig. 2. 4D nuclear tracking analysis of LRP development.**

683 (A–F) The contributions of each cell file of pericycle cells to LRP development
684 visualized by 3D nuclei representation. Nuclei movement and division in the time-lapse
685 data of G–K were tracked and represented using 3D spheres. A, C and E are side views of
686 the LRP; and B, D and F are top-down views. The central cell file of stage I and its
687 lineage are indicated in green; and flanking cell lineages are indicated in orange and red.
688 Blue and light blue indicate additional flanking cell files of stage I. White arrows indicate
689 the central cell file with longitudinal radial cell division at stage V. See also Movie 2.

690 (G–K) Time-lapse image series of LRP development visualized using
691 *pRPS5a::H2B:tdTomato* (red) and *pWOX5::n3GFP* (green). The elapsed time (h:min)
692 from the start of observation and developmental stage are indicated on each panel. See
693 also Movie 3. Scale bar = 50 μ m.

694 (L–P) Front views of digitally sliced images at the indicated positions (white arrows) of
695 G–K.

696 (Q–U) 3D nuclei representation of the QC lineage in the LRP. The QC precursor cell
697 (before *WOX5* expression, yellow) and *WOX5*-positive QC (green) are shown with the
698 surrounding lineage (gray). See also Movie 4.

699 (V–Z) 3D nuclei representation of only the QC lineage from Q–U.

700

701 **Fig. 3. *SCR* and *SHR* expression domains demark the inner and outer LRP layers.**

702 (A) Time-lapse image series of *pSCR::GFP:SCR* (*scr-3*) x WAVE131Y (plasma
703 membrane) initiated from the stage I LRP. GFP::*SCR* was localized in the nuclei. The

704 elapsed time (h:min) from the start of observation is indicated in each panel. See also
705 Movie 5. Scale bars = 50 μ m.

706 (B) Time-lapse image series of *pSHR::SHR:GFP* (*shr-2*) merged with DIC starting from
707 stage I. The fluorescence intensity of SHR:GFP is described by a rainbow look-up color
708 table. The elapsed time (h:min) from the start of observation is indicated in each panel.
709 See also Movies 6, 7. Scale bars = 50 μ m.

710 (C-E) Expression pattern of *SCR* transcriptional reporter (*pSCR::GUS:GFP*) at stage II
711 (C), IV (D) and VI (E). Scale bars = 50 μ m.

712 (F-H) Expression pattern of *SCR* translational reporter (*pSCR::GFP:SCR scr-3*) at stage
713 II (F), IV (G) and VI (H). Scale bars = 50 μ m.

714 (I-K) Expression pattern of *SHR* transcriptional reporter (*pSHR::GUS*) at stage II (I), IV
715 (J) and VI (K). Scale bars = 50 μ m.

716 (L-N) Expression pattern of *SHR* translational reporter (*pSHR::SHR:GFP shr-2*) at stage
717 II (L), IV (M) and VI (N). Scale bars = 50 μ m.

718

719 **Fig. 4. SCR promoted the periclinal cell divisions in the outer layer of stage II LRP.**

720 (A) Time-lapse image series of LRP development in *AUX1-YFP scr-3*. *AUX1-YFP* was
721 used as a plasma membrane marker (green). The elapsed time (h:min) from the start of
722 observation is indicated in each panel. See also Movie 8. Scale bar = 50 μ m.

723 (B) Cell lineage map of the LRP in A. The inner and outer layers of stage II (t = 0:00) are
724 shown in light blue and pink, respectively. Cells derived from the same layer are indicated
725 by the same color.

(C–F) *SCR* promoter activity in the WT and *scr-3* mutant. *pSCR::GUS:GFP* was observed in the second outermost layer of the WT (C, D), and the outermost layer of the *scr-3* mutant (E, F). Because of the large reduction of *SCR* promoter activity in the *scr-3* mutant compared with the WT, we observed the expression using different voltages on a photo multiplier (PMT); 702 V for the WT and 902 V for the *scr-3* with the same laser power (5%). The roots were counterstained with propidium iodide (red). Scale bar = 50 μ m.

Fig. 5. Cell divisions in the outer layer-derived tiers were largely abolished in the *scr-3* mutant.

(A) Cell lineage tree of the central cell at the outer layer of stage II LRP of WT. Cell divisions of the target cell-derived lineage from stage II ($t = 6:00$) were traced in the *pRPS5a::H2B:tdTomato* timelapse data (Fig. 2) for 20 hours.

(B) Cell lineage tree of the central cell in the outer layer of stage II LRP of *scr-3* (*AUX1-YFP scr-3*, Fig. 4). Only one cell division was observed in the cell lineage during 20 hours from stage II. Branch lengths indicated approximate time for cell cycle analyzed by 30 min intervals. Dotted branches indicated the cells out of observed stack.

Fig. 6. *scr* mutation disrupted the normal pattern of QC establishment in LRP.

(A) Time-lapse image series of LRP development in *pWOX5::n3GFP AUX1-YFP* in the *scr-3* background. A nuclear signal indicated *pWOX5::n3GFP* expression (indicated by red arrowheads). The elapsed time (h:min) from the start of observation is indicated in

748 each panel. Scale bar = 50 μ m.

749 (B) Cell lineage map of the LRP of A. The inner and outer layers of stage II (t = 0:00) are
750 colored by light blue and pink respectively. Red indicates inner layer-derived cells that
751 had a *pWOX5::n3GFP* signal.

752

753 **Fig. 7. Schematic model of *Arabidopsis* LR organogenesis.**

754 LR development is biphasic with an initial morphogenesis phase to form basic
755 four-layered LRP followed by meristem formation phase as initially proposed by
756 Laskowski et al. (1995). The transition from bilateral to radial 3D organ shape also
757 coincides with the transition from early morphogenesis to late meristem formation phases.
758 The GRAS-family transcription factor, *SCARECROW* (*SCR*) is specifically expressed in
759 the outer layer of stage II and regulates the formation of precursor cells of QC through
760 *SCR*-mediated periclinal cell divisions (indicated by yellow line at stage III). QC
761 establishment occurs simultaneously with and facilitates the developmental phase
762 transition of LRP at stage V.

763

764 **Supplemental Figures**

765 **Fig. S1. Cellular patterns of the RAM of the PR and emerged LRP.**

766 (A) Confocal image of the primary RAM in *pSCR::GUS:GFP* (endodermis and QC,
767 green) counterstained with PI (cell wall, red). Scale bar = 50 μ m.

768 (B) Schematic representation of the cellular pattern of the RAM in the PR created by
769 tracing cell outlines from A. Cell types are colored according to the legend.

770 (C) Confocal image of the emerged LRP visualized with a plasma membrane-localized
771 fluorescent marker (WAVE131Y, green). Scale bar = 50 μ m.

772 (D) Schematic representation of the cellular pattern of the emerged LRP created by
773 tracing cell outlines from C. Cell colors show the putative cell types based on the
774 information from our observations in this study, and previously reported histological
775 study and marker expression patterns (Malamy and Benfey, 1997).

776

777 **Fig. S2. Original images for 4D nuclei tracking.**

778 Maximum-intensity projections of seven sections at the indicated distance within Z
779 sections at the indicated time points are shown. Circles (4 μ m diameter) drawn in the
780 same colors as in Fig. 2A–F indicate tracked nuclei for 3D representation.

781

782 **Fig. S3. Relative cell positions of the outer layer-derived cell lineages in the WT and**
783 ***scr-3* mutant during LRP development.**

784 Cell positions relative to the initial position (stage II) were analysed from the tracking
785 data of Fig. 5.

786

787 **Fig. S4. *shr* mutation disrupted cell division during LRP development.**

788 (A) Time-lapse image series of LRP development in *AUX1-YFP* in the *shr-2* background.
789 The elapsed time (h:min) from the start of observation is indicated in each panel. Scale
790 bar = 50 μ m.

791 (B) *pSCR::GUS:GFP* in the *shr-2* background. *pSCR::GUS:GFP* was observed in the

792 second outermost layer of the WT, and the outermost layer of the *shr-2* mutant. Because
793 of the large reduction of *SCR* promoter activity in the *shr-2* mutant compared with the WT,
794 we observed the expression using different voltages on a photo multiplier (PMT); 703 V
795 for WT and 903 V for *shr-2* with the same laser power (5%). The roots were
796 counterstained with propidium iodide (red). Scale bars = 50 μ m.

797

798 **Fig. S5. The *scr* mutant created mature LR.**

799 Eleven-day-old seedlings of the WT (Col) and *scr-3* and *shr-2* mutants. Scale bars = 10
800 mm.

801

802 **Supplemental movies**

803 **Movie 1. Time-lapse movie of WAVE131Y x QC25::CFP.**

804 Time-lapse movie of LR primordium development visualized using WAVE131Y (plasma
805 membrane, yellow) and QC25::CFP (QC marker, cyan). The elapsed time (h:min) from
806 the start of observation is indicated at the top. Scale bar = 50 μ m.

807

808 **Movie 2. 3D nuclei representation of LRP development.**

809 Nuclei are distinguished by different colors dependent on the initial cell file. The central
810 cell file (green) provides all cells in the medial section, and flanking cell files (red and
811 orange) contribute to the side parts of the LRP. Additional flanking cell files (blue and
812 light blue) only contribute to a small proportion of the LRP.

813

814 **Movie 3. Time-lapse movie of *pRPS5a::H2B:tdTomato* x *pWOX5::n3GFP*.**

815 Time-lapse movie of LRP development visualized using *pRPS5a::H2B:tdTomato* (red)
816 and *pWOX5::n3GFP* (green). The elapsed time (h:min) from the start of observation is
817 indicated at the top. Scale bar = 50 μ m.

818

819 **Movie 4. 3D nuclei representation of the QC cell lineage.**

820 QC precursor cells (yellow) were produced by periclinal cell division at the outer layer of
821 stage II, and then acquired QC identity (green). After QC marker expression, the QC
822 underwent longitudinal radial cell division to create four QC cells.

823

824 **Movie 5. Time-lapse movie of *pSCR::GFP:SCR* (*scr-3*) x WAVE131Y.**

825 Time-lapse movie of *pSCR::GFP:SCR* (nuclei, green) x WAVE131Y (plasma membrane,
826 green) in the *scr-3* mutant background. The elapsed time (h:min) from the start of
827 observation is indicated at the top. Scale bar = 50 μ m.

828

829 **Movie 6. Time-lapse movie of *pSHR::SHR:GFP* (*shr-2*) merged with DIC.**

830 The fluorescence intensity of SHR:GFP was described by a rainbow look-up color table.

831 The elapsed time (h:min) from the start of observation is indicated at the top. Scale bar =
832 50 μ m.

833

834 **Movie 7. Time-lapse movie of *pSHR::SHR:GFP* (*shr-2*).**

835 The GFP channel only from Movie 6. Fluorescence intensity of SHR:GFP was described

836 by a rainbow look-up color table. The elapsed time (h:min) from the start of observation
837 is indicated at the top. Scale bar = 50 μ m.

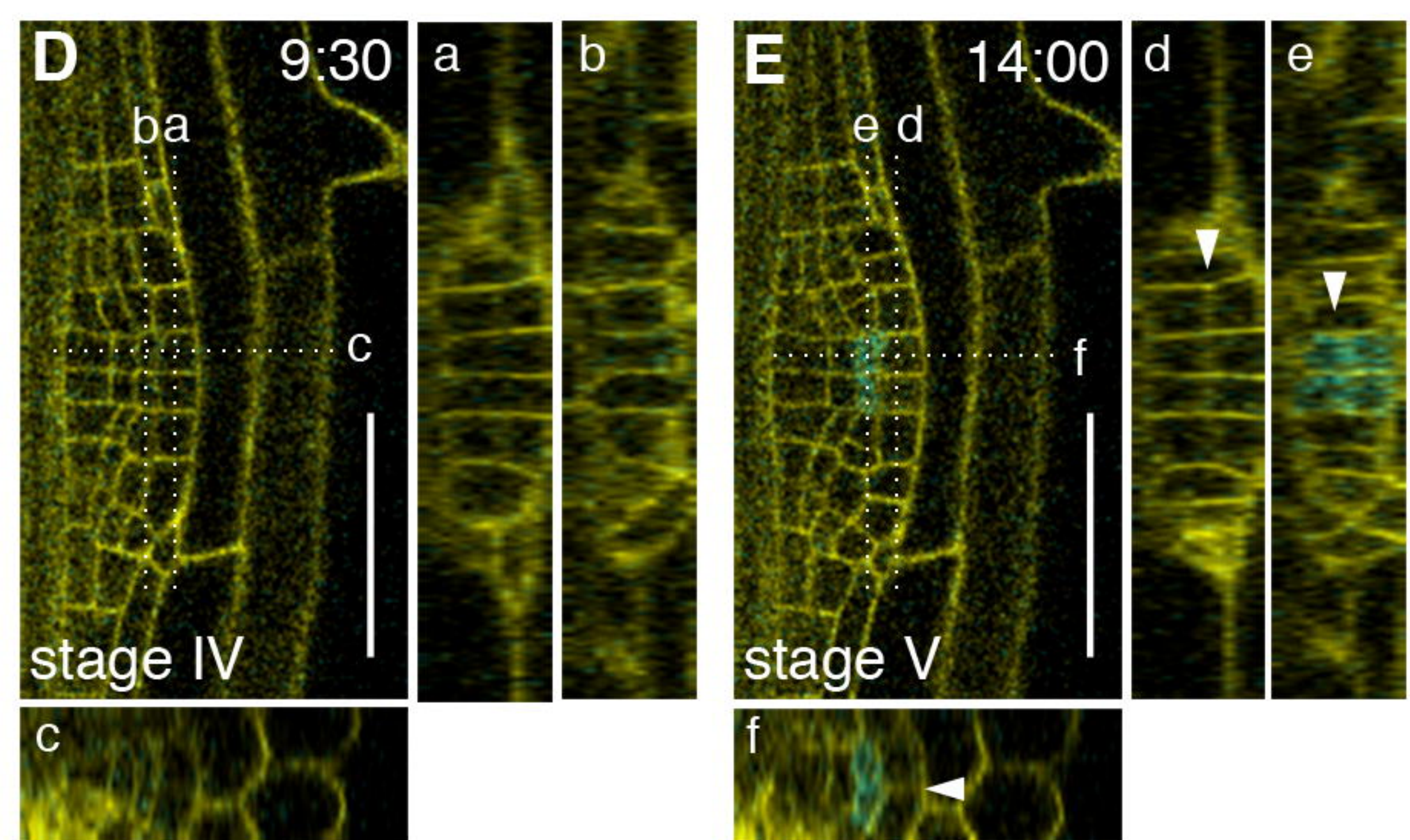
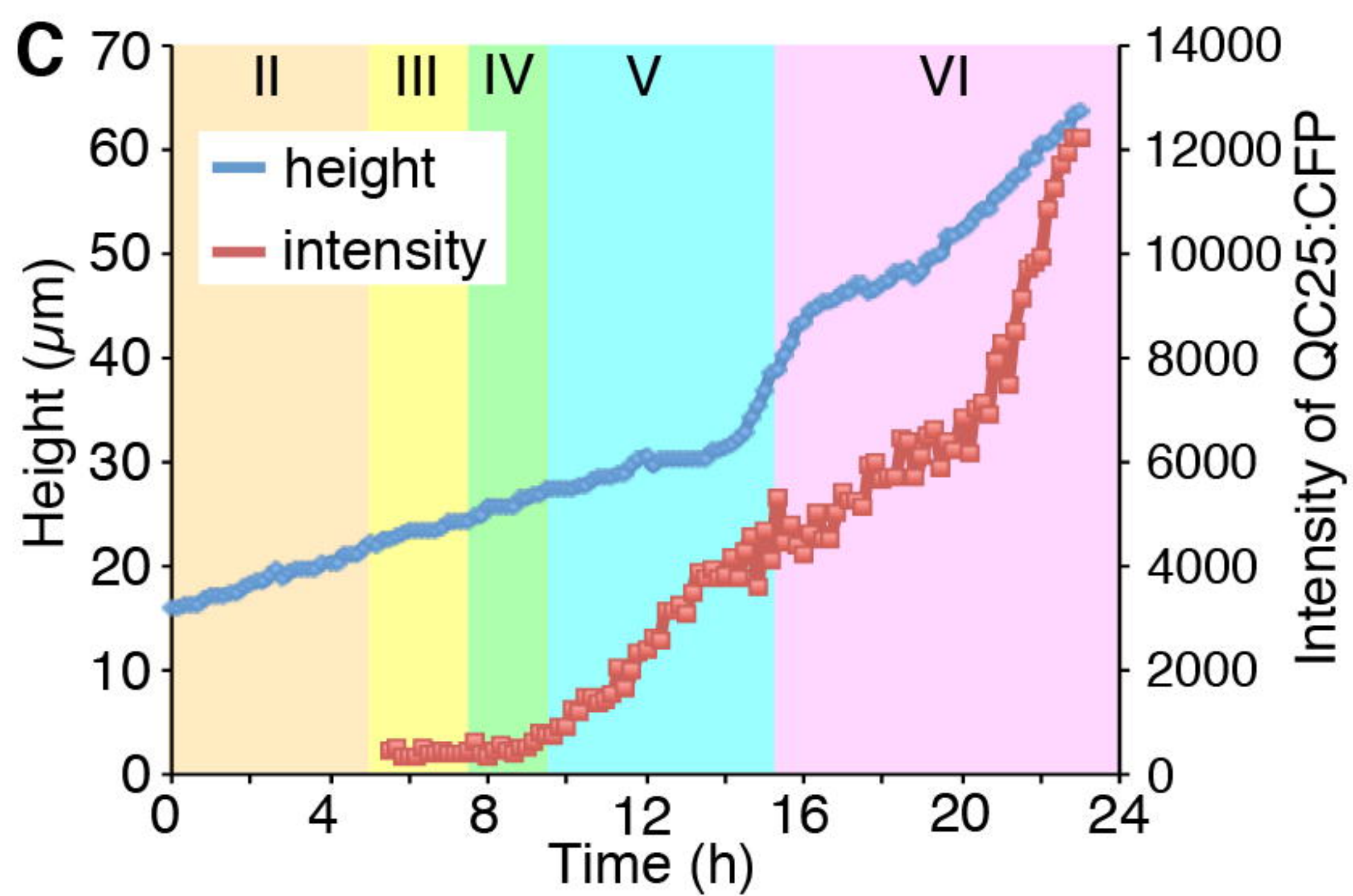
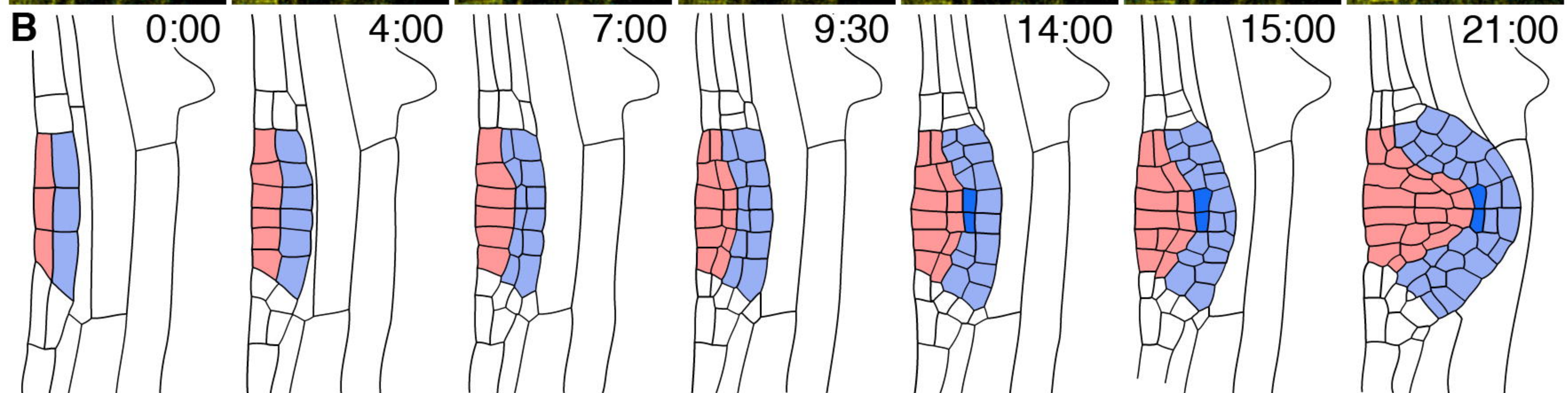
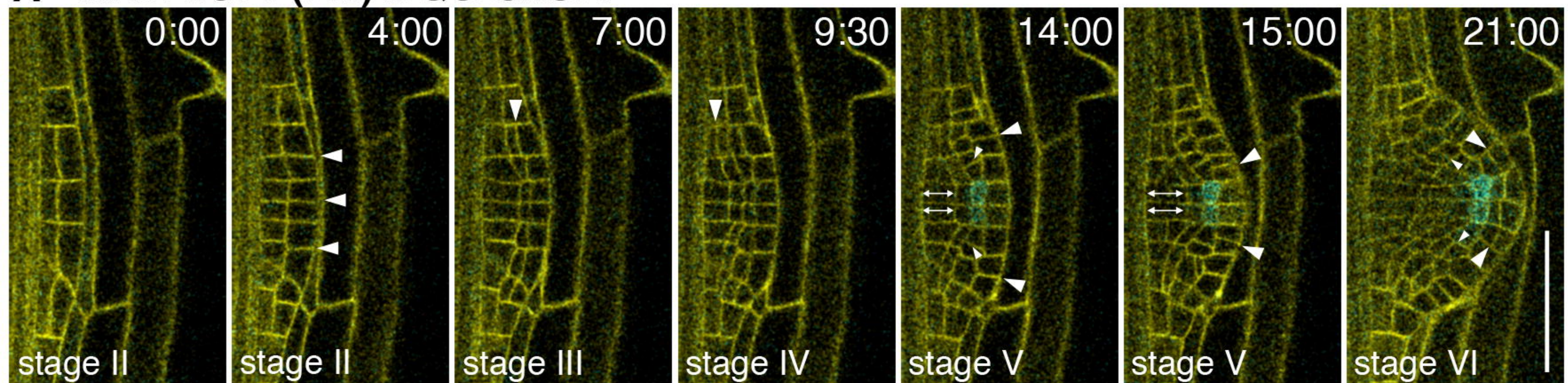
838

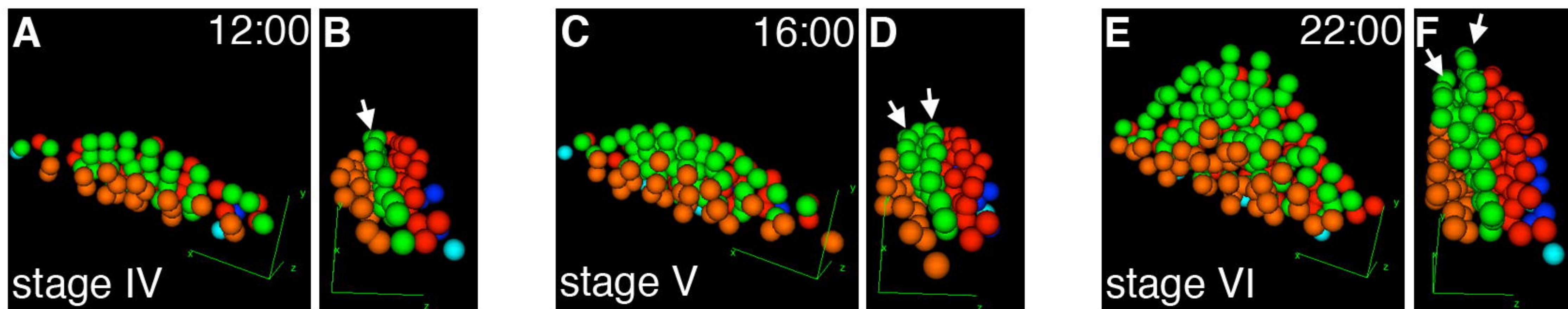
839 **Movie 8. Time-lapse movie of LRP development in *AUX1-YFP_{scr-3}*.**

840 The elapsed time (h:min) from the start of observation is indicated at the top. Scale bar =
841 50 μ m.

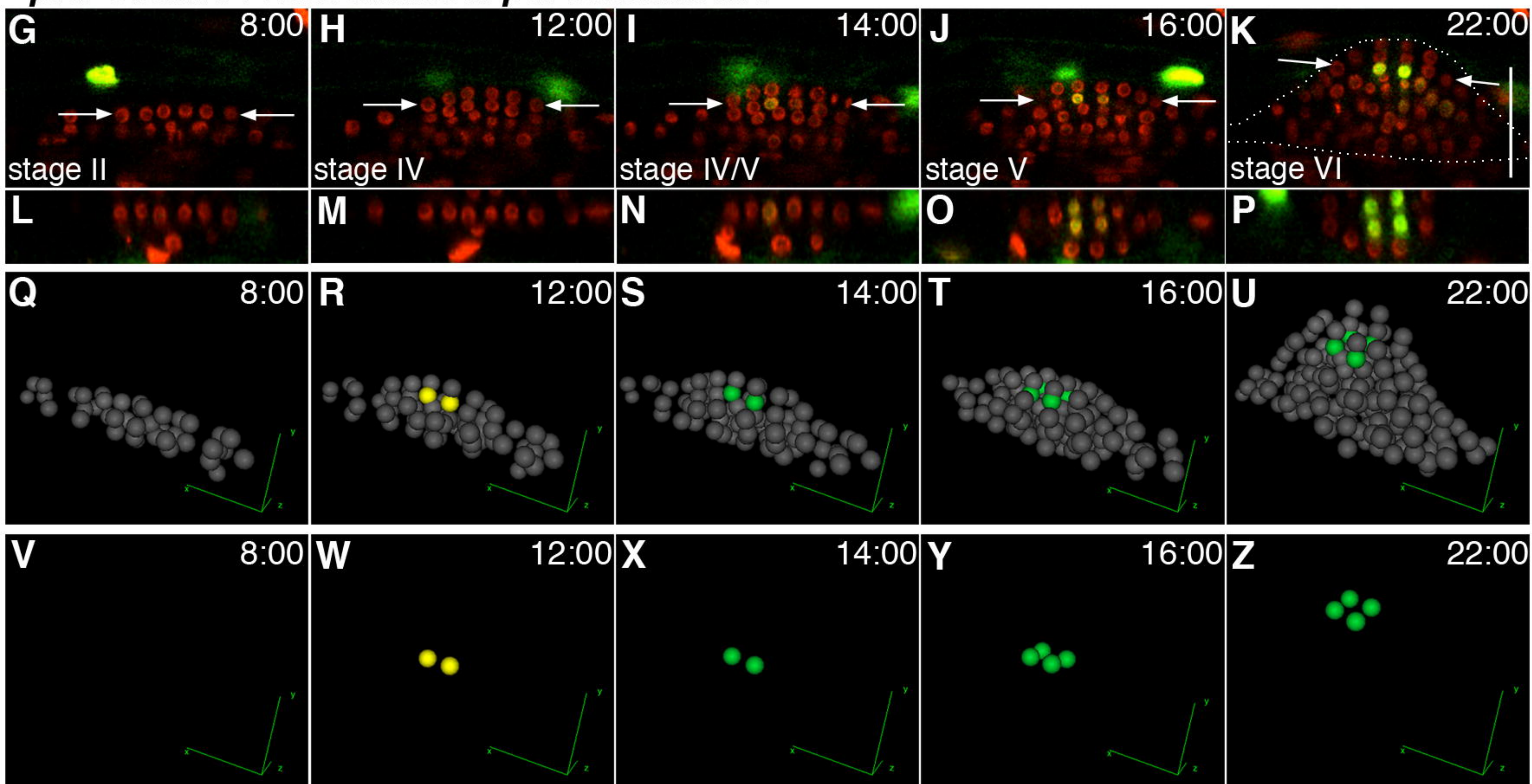
842

A *WAVE131Y* (PM) x *QC25::CFP*

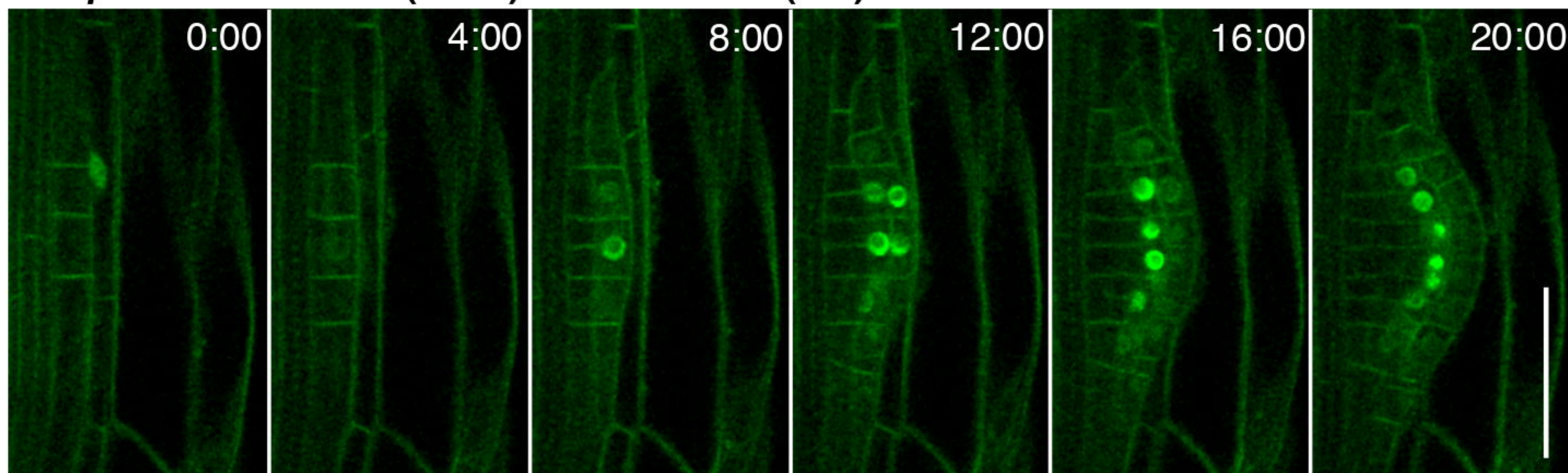




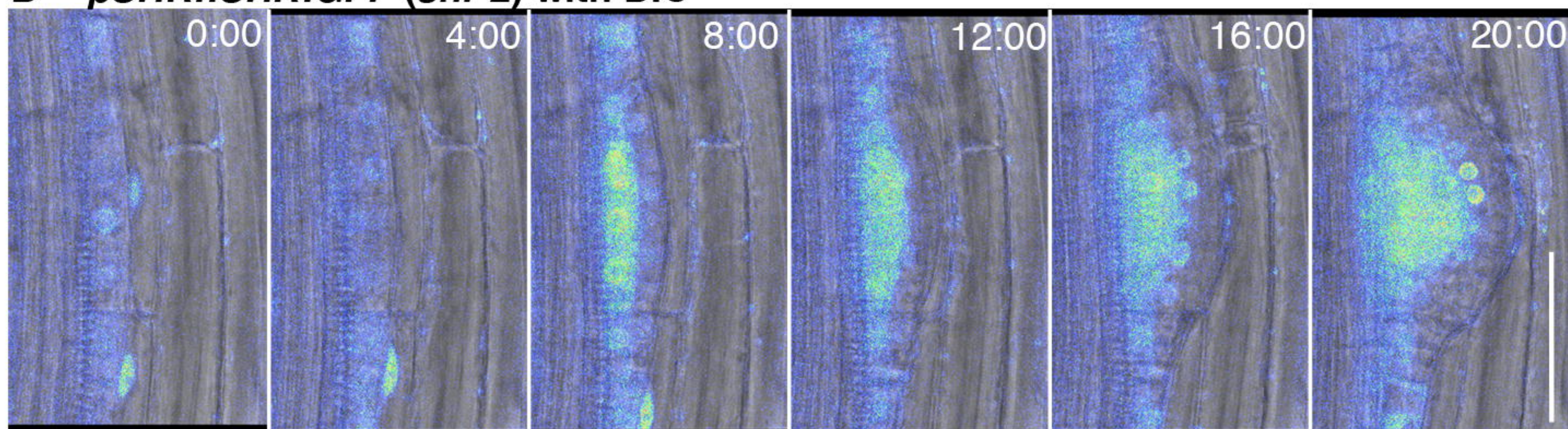
pRPS5a::H2B:tdTomato x pWOX5::n3GFP



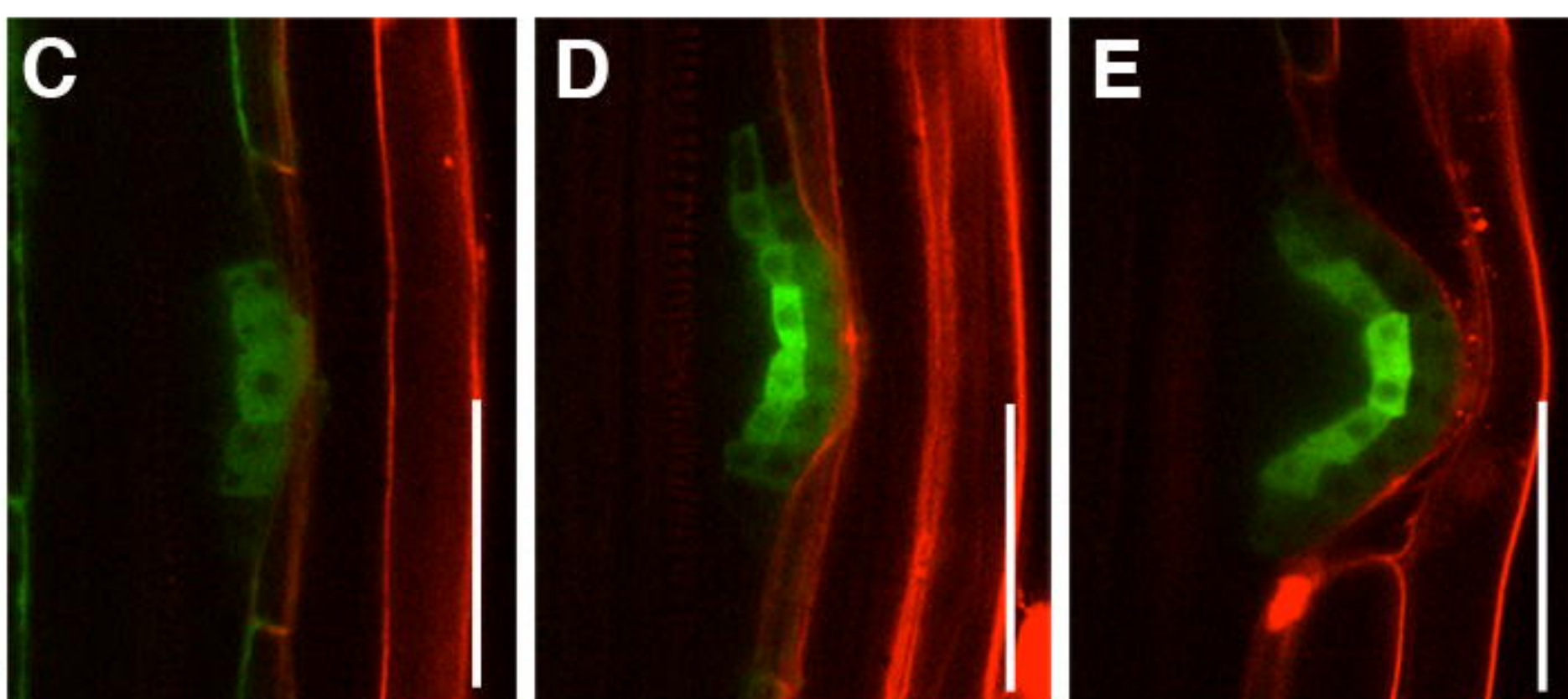
A *pSCR::GFP:SCR (scr-3) x WAVE131Y (PM)*



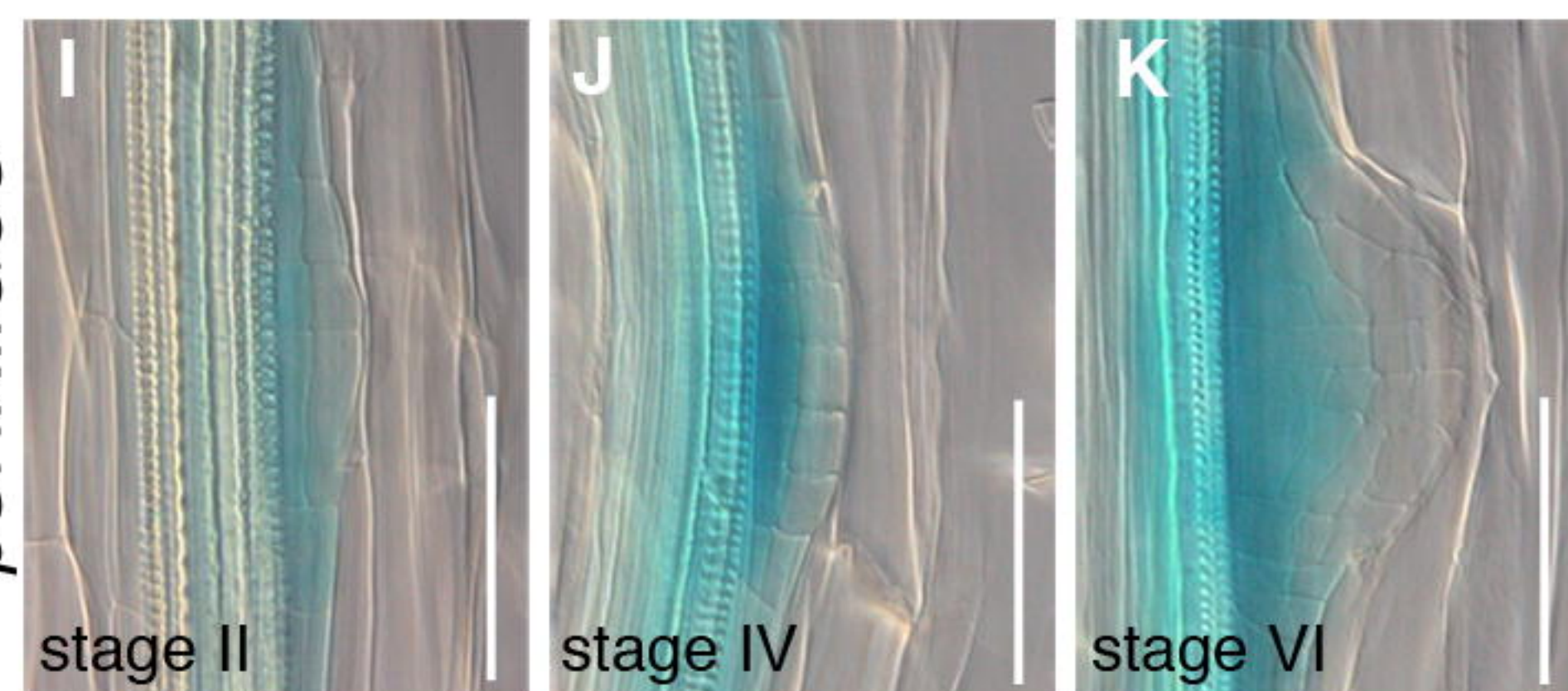
B *pSHR::SHR:GFP (shr-2) with DIC*



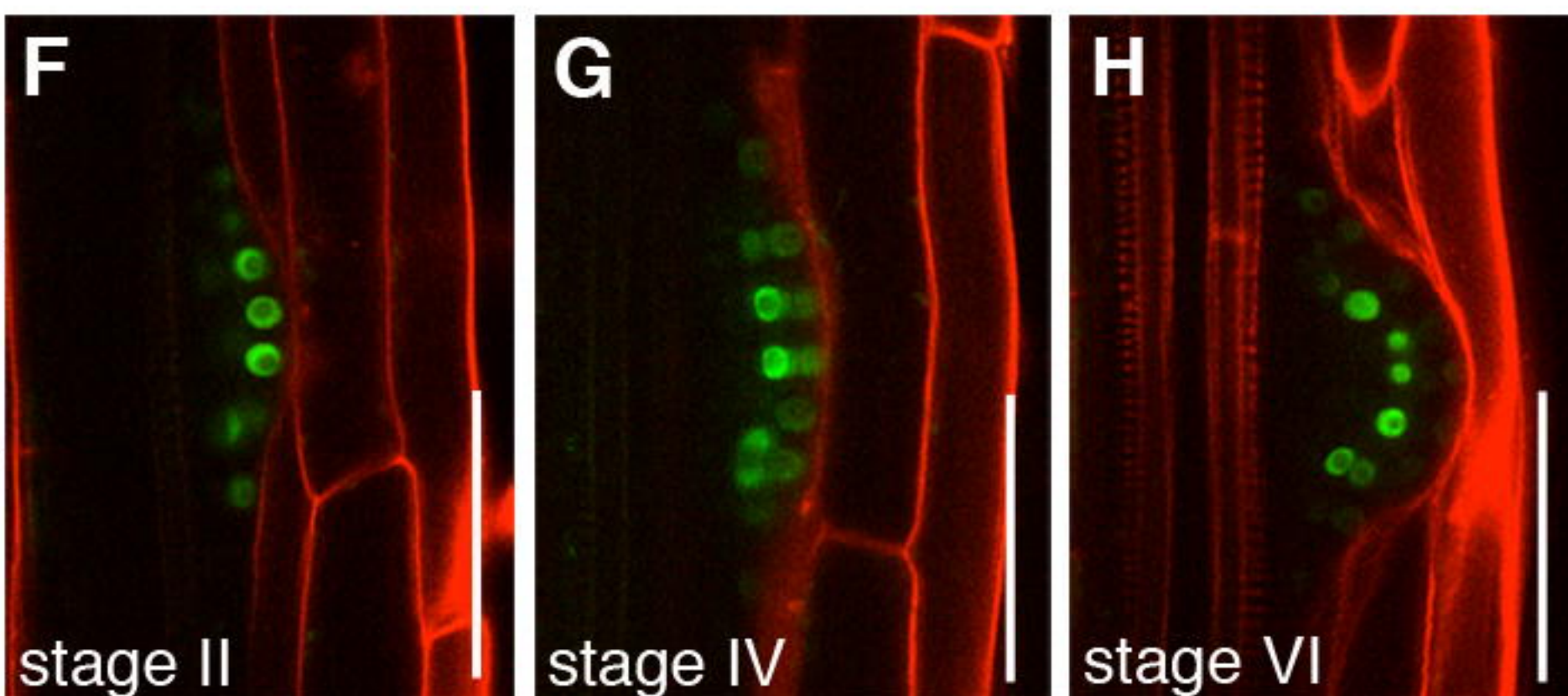
pSCR::GUS:GFP



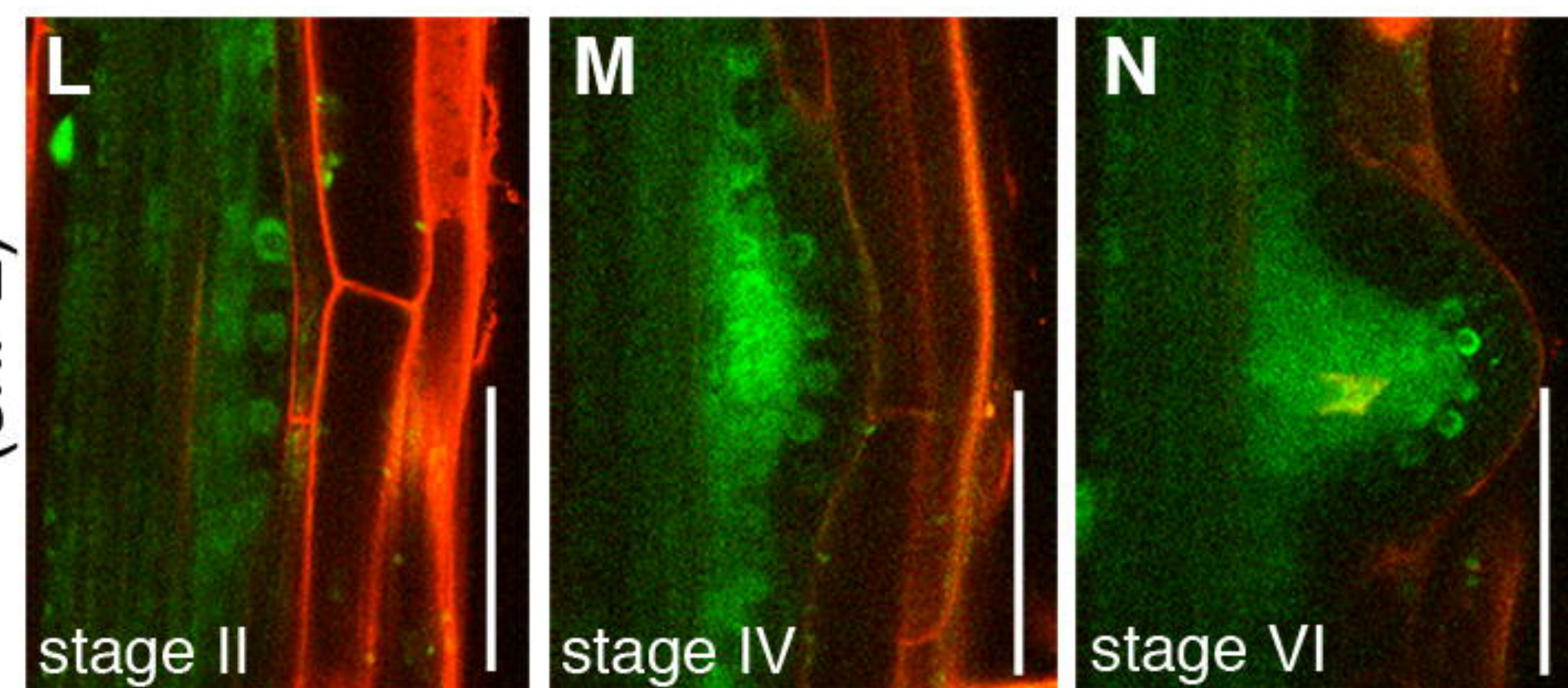
pSHR::GUS



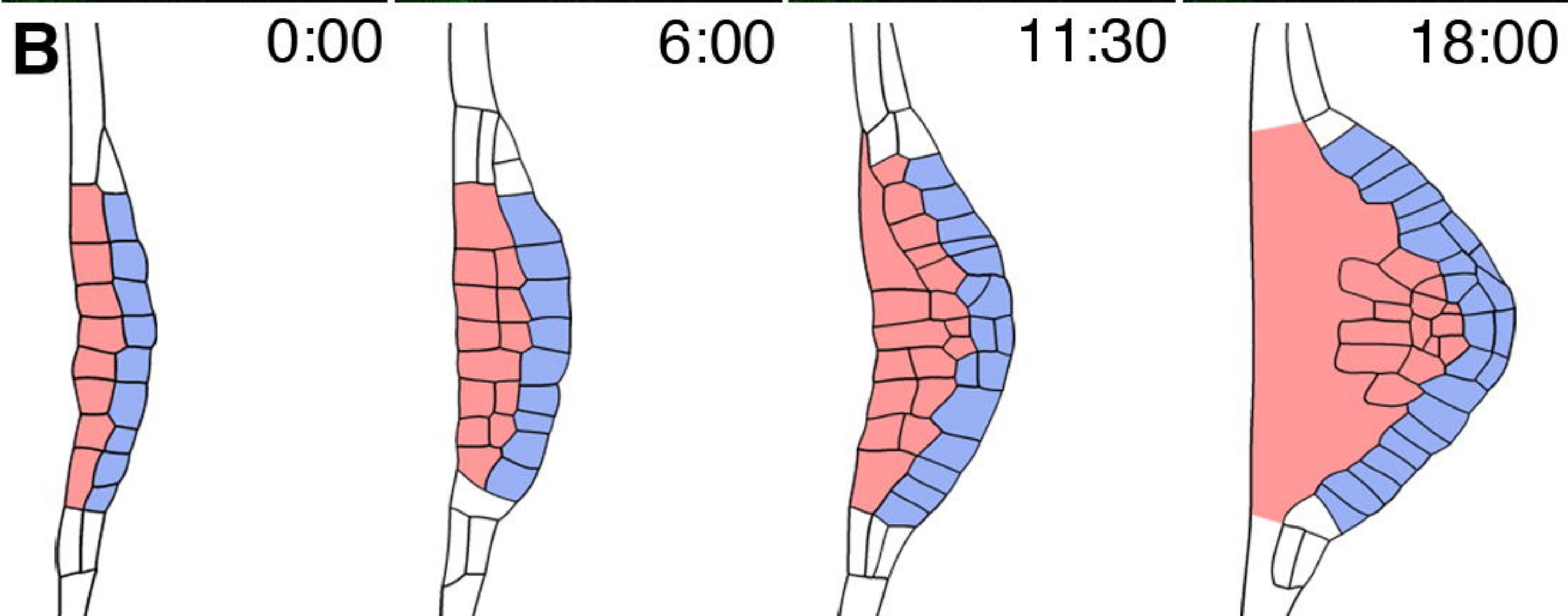
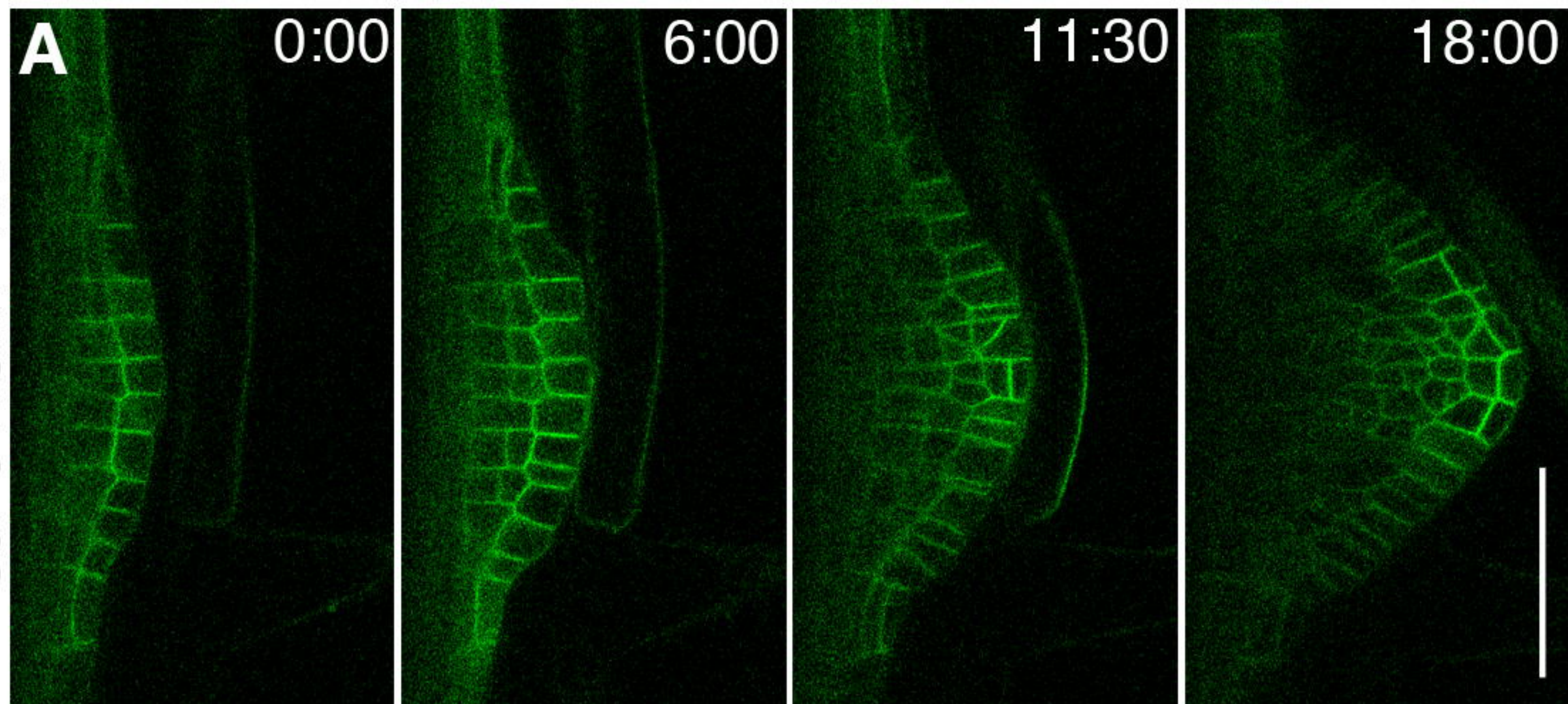
pSCR::GFP:SCR (scr-3)



pSHR::SHR:GFP (shr-2)



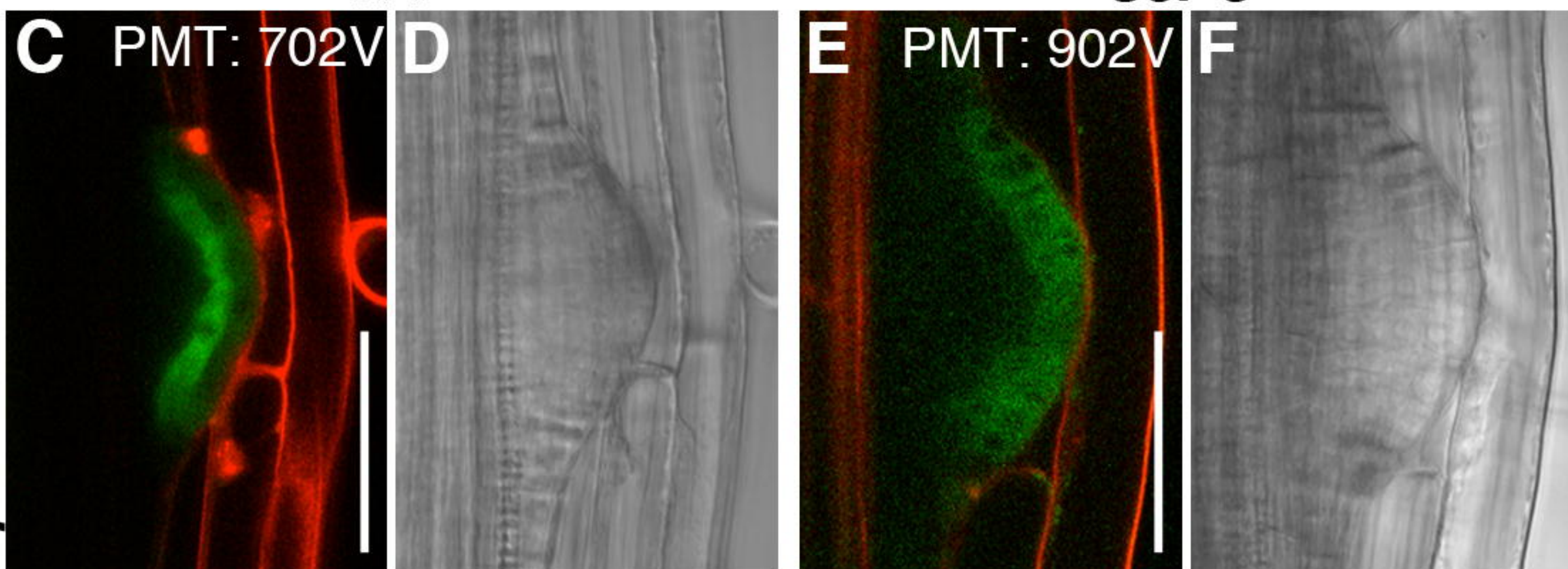
scr-3 AUX1-YFP



WT

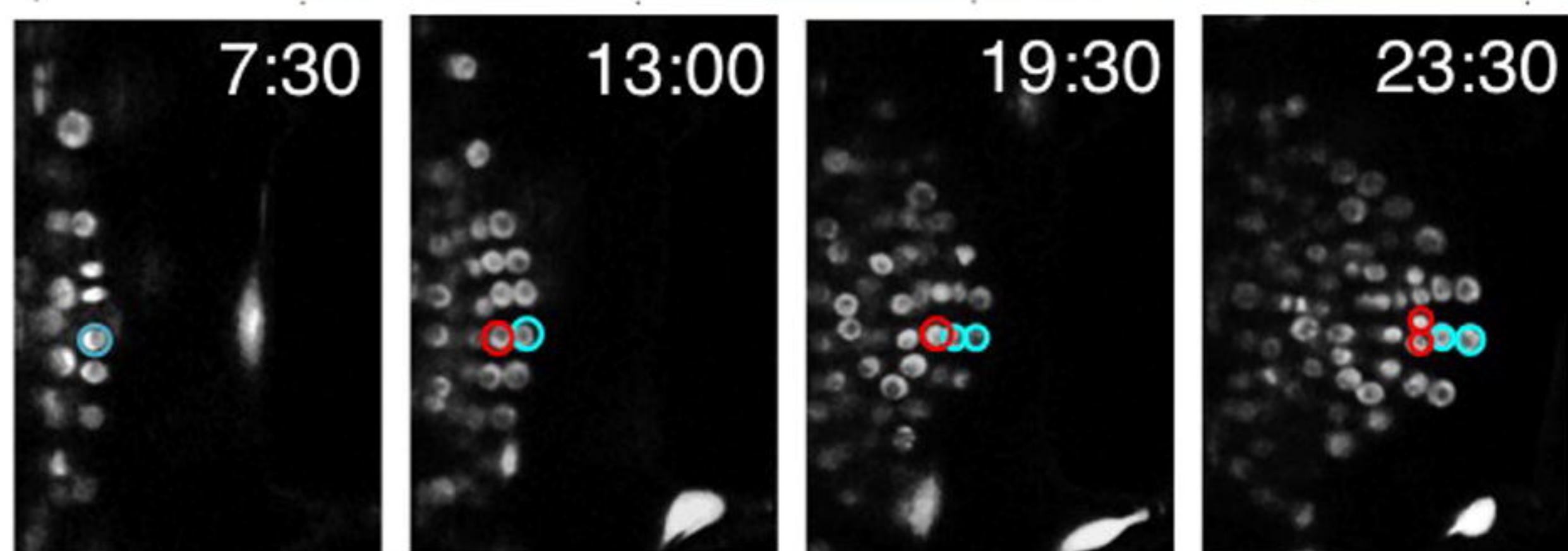
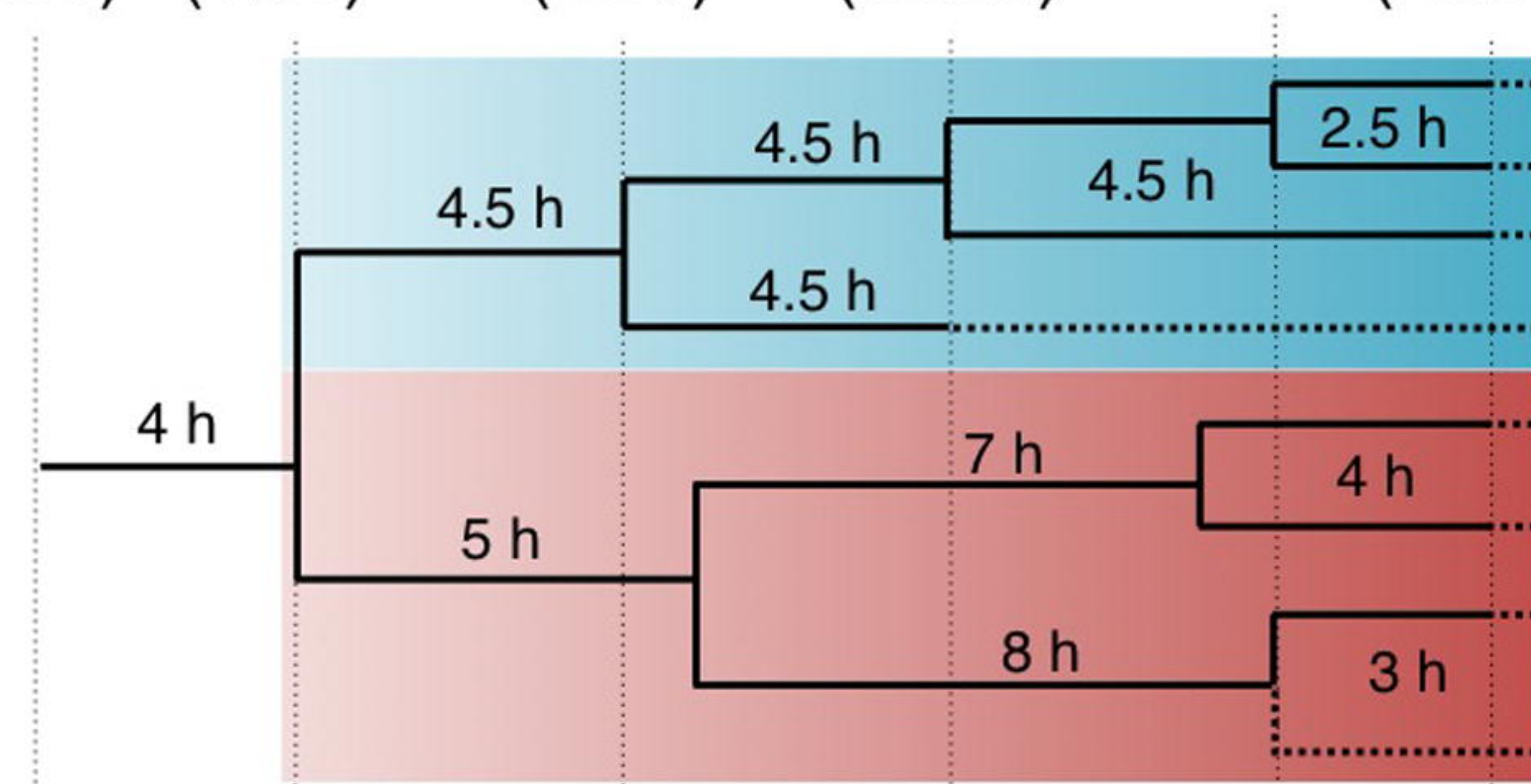
scr-3

pSCR::GUS::GFP



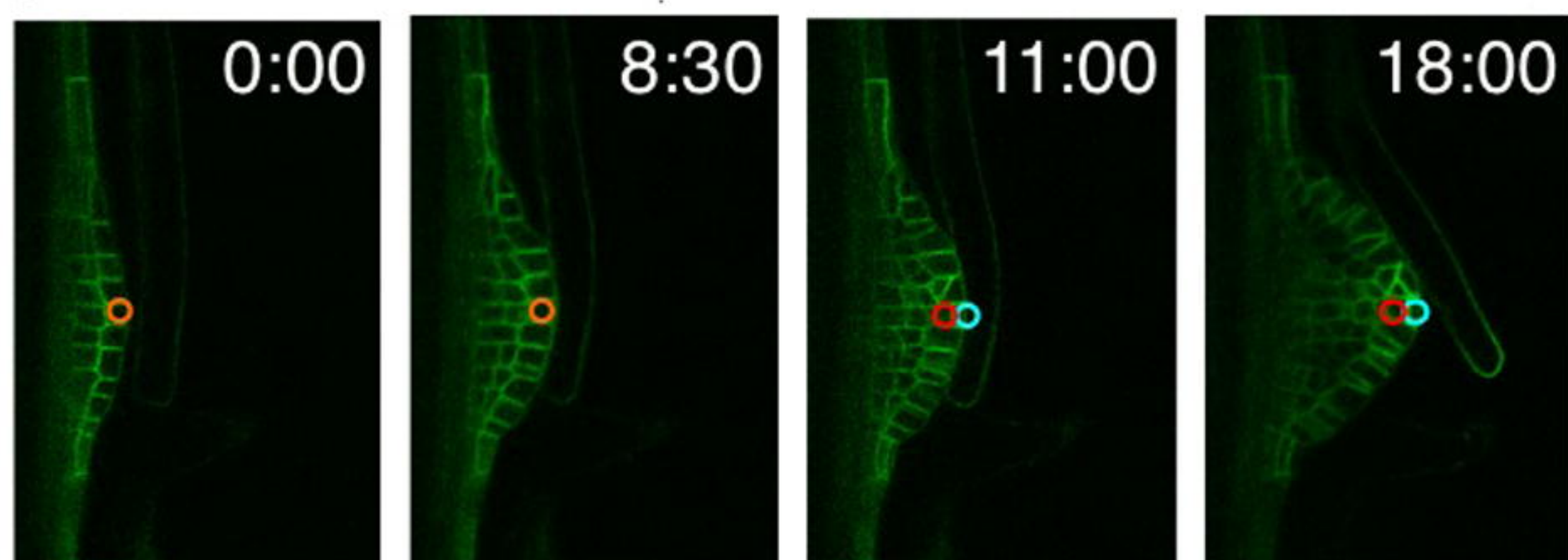
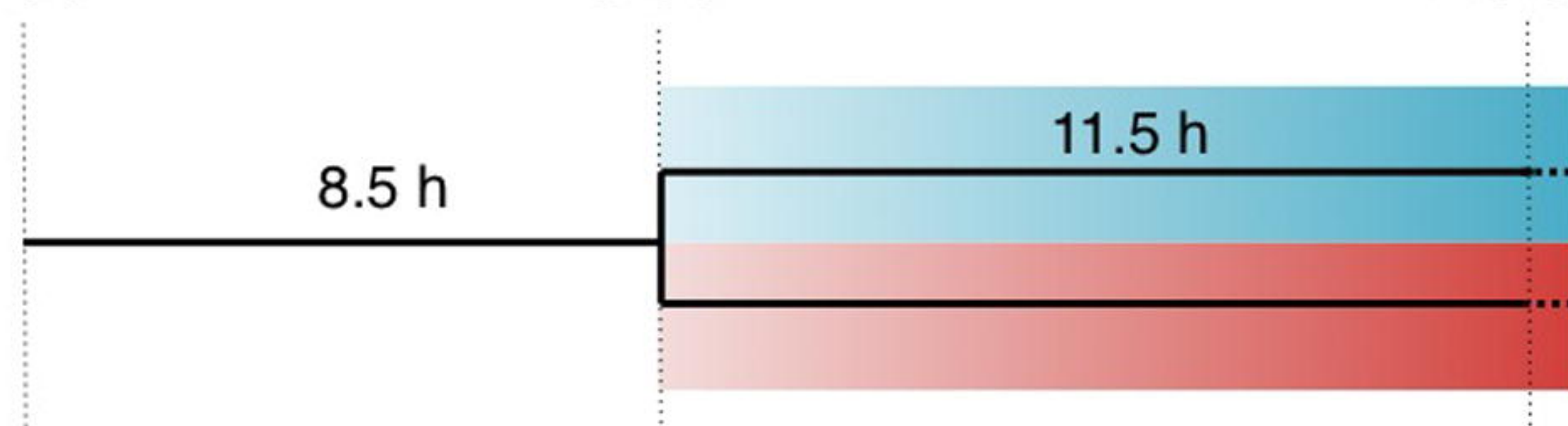
A WT (*pRPS5a::H2B:tdTomato*)

6:30 (0:00) 10:30 (4:00) 15:00 (9:30) 19:30 (13:00) 26:30 (20:00)

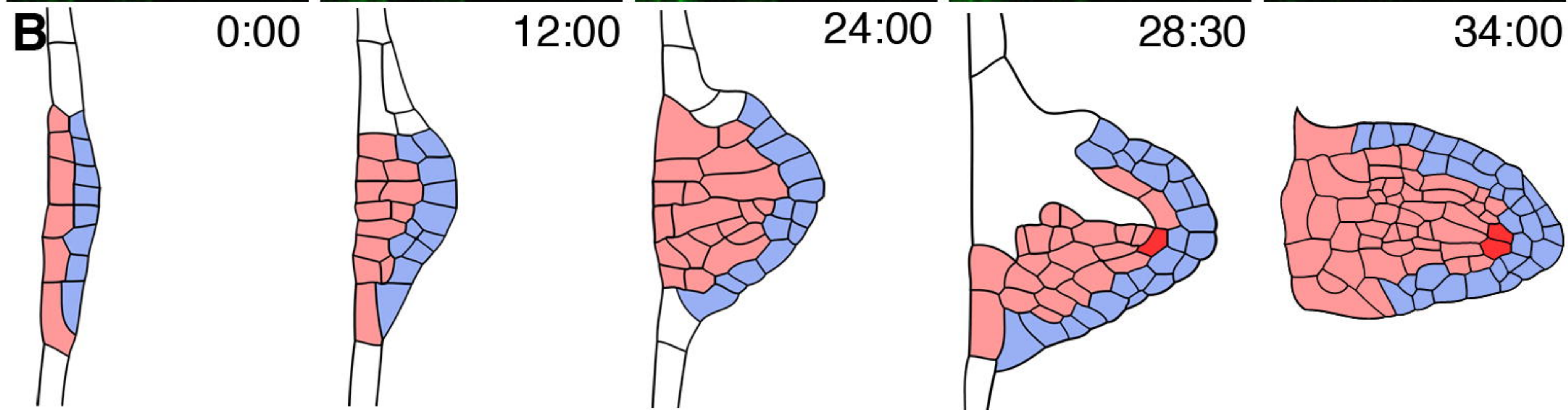
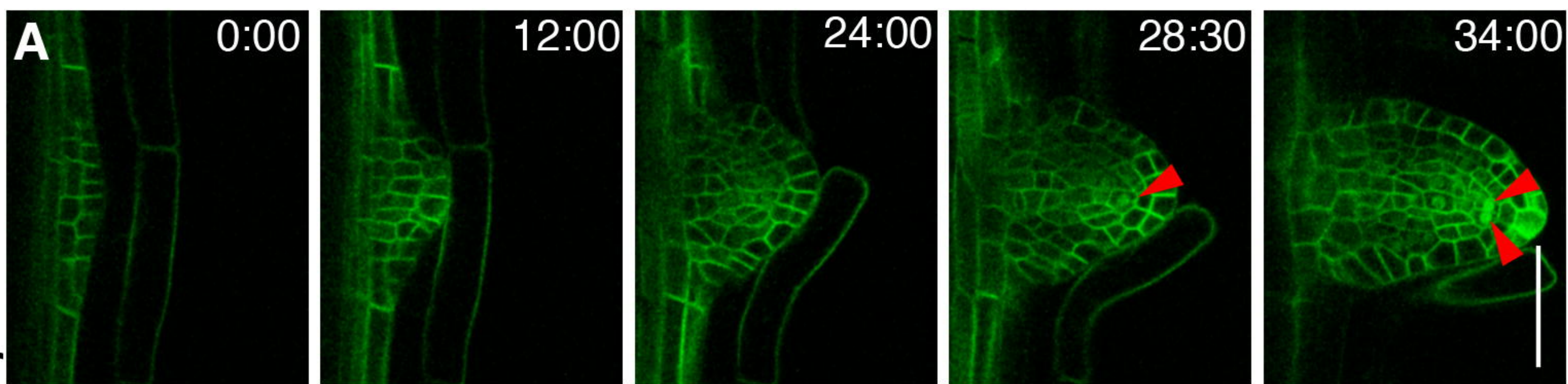


B *scr-3* (*AUX1-YFP scr-3*)

0:00 8:30 20:00



scr-3 AUX1-YFP
pWOX5::n3GFP



early morphogenesis phase

meristem formation phase

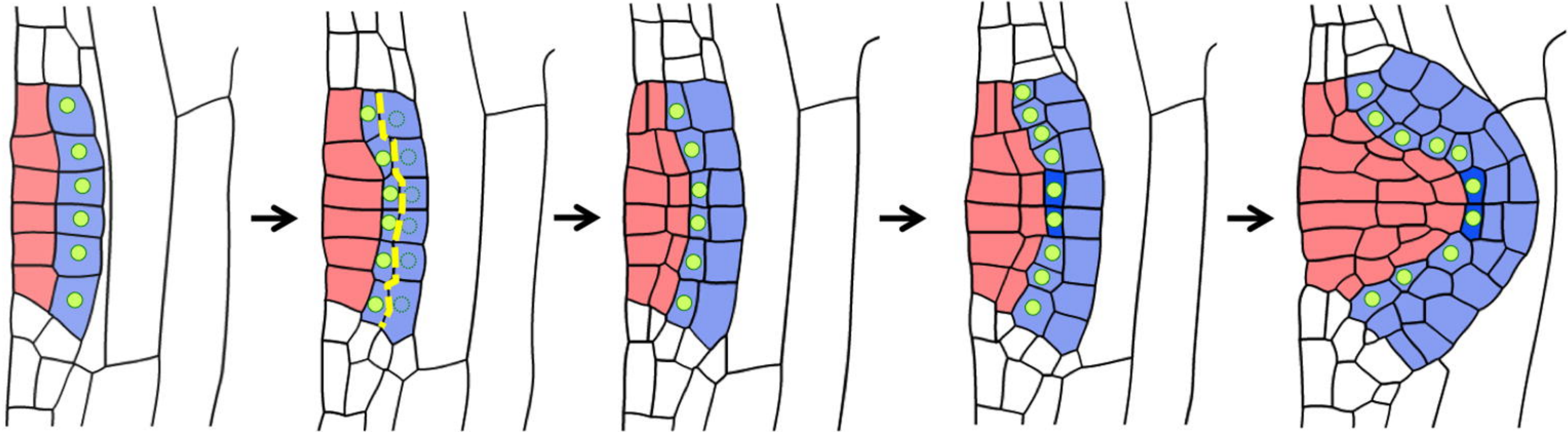
stage II

stage III

stage IV

stage V

stage VI



outer layer-specific
expression of *SCR*

the second periclinal divisions
mediated by *SCR*
(yellow line)

QC specification
(dark blue)

meristem organization

● *SCARECROW* (*SCR*)

■ QC marker-positive cells

■ outer layer-derived cells

■ inner-derived cells